Kaya, N., Hisarlı, Z. M., Nowaczyk, N., Makaroğlu, Ö. (2023): The Variation of Geomagnetic Field Intensity in Central Anatolia During the Neogene-Quaternary Period. - Geophysical Journal International, 233, 3, 1708-1726.

https://doi.org/10.1093/gji/ggad005

Geophysical Journal International
Geophys. J. Int. (2023) **233,** 1708–1726
Advance Access publication 2023 January 06
GJI Geomagnetism, Rock Magnetism and Palaeomagnetism
https://doi.org/10.1093/gji/ggad005

The variation of geomagnetic field intensity in Central Anatolia during the Neogene-Quaternary period

Nurcan Kaya [1] Z. Mümtaz Hisarlı [1] Norbert R. Nowaczyk [2] and Özlem Makaroğlu [1]

[1] *İstanbul University-Cerrahpaşa, Faculty of Engineering, Department of Geophysical Engineering,* 34500 *Büyükçekmece, İstanbul, Türkiye. E-mail: nurcan.kaya@iuc.edu.tr*

[2] *Helmholtz Centre Potsdam, German Research Centre for Geosciences GFZ, Section* 4.3 – *Climate Dynamics and Landscape evolution,* 14473 *Potsdam, Germany*

Accepted 2022 December 19. Received 2022 December 15; in original form 2022 June 3

SUMMARY

A detailed palaeointensity study was performed using the modified Thellier method on 18 Quaternary and Neogene volcanic units, ages ranging from 0.08 to 5.98 Ma, in Central Anatolia, Turkey. Robust data, which were estimated from 12 lava units in the study area, significantly increase the database of palaeomagnetic data, directions and absolute palaeointensity for the Anatolian region covering the time window back to ∼6 Ma. Previous studies sensitively dated the samples, except for one site dated in this study. The palaeointensity (VDM) value from the upper Miocene site estimated as $48.6 \pm 9.2\ \mu$T ($10.1 \times 10^{22} \pm 1.9$ Am^2) fits well into the Neogene VDM range in the data archives. For Pliocene samples with an age of 4.7 Ma, the palaeointensity was calculated to be $21.0 \pm 4.7\ \mu$T. For these samples, an inclination of $+42.9^\circ$ was determined, and together with the results of low palaeointensity and normal polarity, this corresponds to the Nunivak or Sidufjall subchrons. These are normal polarity chrons within the Gilbert Chron which predominantly has reversed polarity. Palaeodirectional data and field strength with age between 0.08 and 2.57 Ma clearly showed the Brunhes and Matuyama Chrons in the Pleistocene. Three new data with $25.0 \pm 7.9\ \mu$T (age 1.84 Ma), $59.7 \pm 8.2\ \mu$T (age 2.15 Ma) and $79.6 \pm 19.3\ \mu$T (age 2.57 Ma) from the early Pleistocene period significantly contribute to global data archives, which lack palaeointensity data from similar latitude range. The average VDM values for nine Pleistocene sites were calculated to be $51.5 \pm 16.4\ \mu$T ($10.3 \times 10^{22} \pm 3.7$ Am^2). According to the comparison of our data with the palaeointensity database, field model record and previous studies of the Pleistocene, significantly high field strength obtained from Central Anatolia, located in the Northern Hemisphere, could have occurred due to asymmetry between the Northern and Southern Hemispheres during the Pleistocene.

Key words: Central Anatolia; Palaeointensity; Palaeomagnetism; Rock and mineral magnetism; Asia; Neogene-Quaternary.

1 INTRODUCTION

The geomagnetic field is the only physical property of planet Earth that is continuously recorded during geological times (Tarling 1971). Determination of the long-term changes in the magnetic field and understanding its dynamics have been research topics for many years in palaeomagnetism. Recently, geomagnetic field models created with data including the variation of the Earth's magnetic field strength and direction have been frequently used to improve our understanding of the profound inner evolution of the Earth, such as the fluid dynamics of the liquid outer core or polarity reversals. An analysis of the dipole contribution of the magnetic field derived from spherical harmonic models based on field data from geomagnetic observatories shows that the dipole moment has decreased at least since the early 19th century. Currently, it is decreasing at a rate of about 5.8 per cent per century (Leaton & Malin 1967; McDonald & Gunst 1968; Langel 1987). If it continues to decrease at this rate, the dipole moment of the Earth's magnetic field will vanish completely in approximately 2000 yr (Bloxham 1986; Finlay *et al.* 2016). For this reason, determining the variability in geomagnetic field strength throughout the geological past is essential to predict the future trends in the behaviour of the present geomagnetic field. Furthermore, there are unanswered questions regarding the non-dipole field throughout geological time. For example, the

South Atlantic Anomaly (SAA; Korte & Constable 2005; Gubbins *et al.* 2006; Korte *et al.* 2011; Aubert 2015; Finlay *et al.* 2016) and hemispheric asymmetry (Cromwell *et al.* 2013; Asefaw *et al.* 2021; Tauxe *et al.* 2022). SAA is a significant departure from the geocentric axial dipole (GAD) field observed in the present day, and measurements over historical and archaeological timescales indicate that non-axial-dipole effects persist at least over the last 10 kyr. Global paleodirectional data in the last 5 Myr shows that the GAD is more dominant than the non-GAD structure of the geomagnetic field. However, the palaeointensity database for the same period does not support this situation. Higher palaeointensity values are expected at higher latitudes in the GAD area. However, the current database shows that palaeointensity is independent of latitude. Asefaw *et al.* (2021) conducted a palaeointensity study in Antarctica to investigate the reason for this. The palaeointensity values they obtained were weaker than expected. A similar study was carried out by Tauxe *et al.* (2022) in northern Israel (33°N latitude). The palaeointensity values obtained with Pleistocene data in northern Israel were higher than Iceland in the north and lower than Hawaii in the south. These non-symmetrical changes in the GAD were explained as being due to the long-lived non-axial dipole terms in the geomagnetic field. The reliability of these results depends on the quality of palaeointensity studies and whether a sufficient number of temporal samples were examined.

The Earth's magnetic field directions are easily obtained with palaeomagnetic studies. In contrast, it is difficult to obtain reliable absolute palaeointensity data due to laboratory measurements and data interpretation difficulties. The absolute palaeointensity data obtained from volcanic and archaeological samples recently are listed in the PINT database (Bono *et al.* 2021). The PINT database clearly shows that palaeointensity data are intensely concentrated during the Holocene, whereas data from the Pleistocene and Miocene have relatively low concentration. The distribution of palaeointensity data from Europe and Asia is also characterized by a remarkable gap in data from Turkey, with only a few palaeointensity data points from the Holocene period obtained from sedimentary, volcanic and archaeological samples from Anatolian sites (Bucha & Mellaart 1967; Sarıbudak & Tarling 1993; Sayın & Orbay 2003; Ertepınar *et al.* 2012, 2014, 2020; Makaroğlu *et al.* 2020; Makaroğlu, 2021). In addition, only one study was performed on volcanic rocks in Turkey with ages of 0–6 Ma (Baydemir *et al.* 2012). Baydemir *et al.* (2012), who studied 12 volcanic sites around the Eastern Anatolian region with ages of 0.1–5.5 Ma, obtained palaeointensity values lower than the present-day field (47 μT). A detailed palaeointensity study of volcanic rocks from Anatolia was performed within the scope of a PhD thesis by Kaya (2020).

Compilations of global and regional palaeointensity data are critical for testing the dynamics of Earth's magnetic field, such as the previously mentioned present field intensity decrease (Leaton & Malin 1967; McDonald & Gunst 1968; Langel 1987); SAA (Korte & Constable 2005; Gubbins *et al.* 2006; Korte *et al.* 2011; Aubert 2015; Finlay *et al.* 2016; Engbers *et al.* 2022) and hemispheric asymmetry hypothesis (Tauxe *et al.* 2022). An intense compilation is only possible by increasing the number of intensity and directional data about the Earth's magnetic field in time and space at high resolution.

Therefore, in this research, a palaeointensity study was performed on rocks from eighteen Quaternary–Neogene volcanic sites located in central Anatolia (38°N) to increase palaeointensity data in Anatolia and test hemispheric asymmetry. The new results were compared with previous palaeointensity data obtained from similar age intervals and then to filtered data from the PINT database (Bono *et al.* 2021) and PADM2M (Ziegler *et al.* 2011). Finally, dynamic changes in Earth's magnetic field were also discussed regarding our data, such as reversals during the last 6 Ma and hemispheric asymmetry during the Pleistocene period.

2 GEOLOGICAL SETTING

Neogene–Quaternary volcanism in Central Anatolia was triggered by continental collision of the Afro-Arabian and Eurasian plates (Fig. 1). The Central Anatolian Plateau corresponds to an area bounded by two faults, the Tuz Gölü and Ecemiş faults, located between Quaternary stratovolcanoes, such as Hasan Mountain and Mount Erciyes. Lava domes, lava flows, cones, craters, volcanic tuff and agglomerates formed during upper Tertiary to Quaternary volcanic activity in the region between Konya and Kayseri within an SW–NE-oriented belt (Figs 1 and 2). They crop out in the Erenlerdağı-Alacadağ massif, in Karadağ, around Karapınar, in the Hasandağ-Erciyesdağ volcanic area and around Nevşehir. The high volcanic cones of Hasan Mountain and Mount Erciyes, small craters around Karapınar and Nevşehir and sprinkled tuffs and fairy chimneys of Göreme (Ürgüp) region are natural remnants of this young volcanic activity in Central Anatolia (Fig. 1; Beekman 1966; Pasquarè 1968; Innocenti *et al.* 1975; Le Pennec *et al.* 1994; Toprak 1998). The products of volcanic activity in Central Anatolia are generally characterized by calc-alkaline andesite, dacite, rhyodacite, alkaline basalt, trachyte and phenolate composition. The ages of volcanic rocks in the study area vary between 13.7 and 0.0019 Ma (Innocenti *et al.* 1975; Besang *et al.* 1977; Ercan *et al.* 1992; Bigazzi *et al.* 1993; Mues-Schumacher & Schumacher 1996; Platzman *et al.* 1998; Doğan 2011; Aydar *et al.* 2013).

3 METHODS

3.1 Sampling and dating

For this study, a total of 450 standard palaeomagnetic samples were collected with a gasoline-powered portable drill and oriented using a magnetic compass from eighteen sites (from NK1 to NK18; Fig. 2). Fourteen of these sites (NK1, NK2, NK3, NK4, NK5, NK6, NK8, NK9, NK10, NK11, NK12, NK13, NK14 and NK16) were in Quaternary volcanoes, whereas the other four sites (NK7, NK15, NK17 and NK18) were located in a Neogene volcanic area (Fig. 2). The site coordinates are listed in Table 1. The measurements were performed at Yılmaz İspir Palaeomagnetic Laboratory in Istanbul University-Cerrahpaşa (Istanbul, Turkey), except hysteresis measurements, which were done at the Laboratory for Palaeo- and Rock magnetism of Helmholtz-Centre Potsdam GFZ, Germany.

Seventeen sites were dated by previous studies using Ar/Ar and K/Ar age analyses (Mues-Schumacher & Schumacher 1996; Platzman *et al.* 1998; Doğan 2011; Aydar *et al.* 2013; Table 1), whereas one site (NK6) was dated in this study by K/Ar age analysis performed at Actlabs in Canada (Tables 1 and 2). The sample from site NK6 was dated from whole rock using an MI-1201 mass spectrometer. For age calculations, the international values of constants were used as follows:

$\lambda_K = 0.581 \times 10^{-10}$ yr^{-1}, $\lambda_{\beta^-} = 4.962 \times 10^{-10}$ yr^{-1}, $^{40}K = 0.01167$ (atm per cent). The detailed result is given in Table 2.

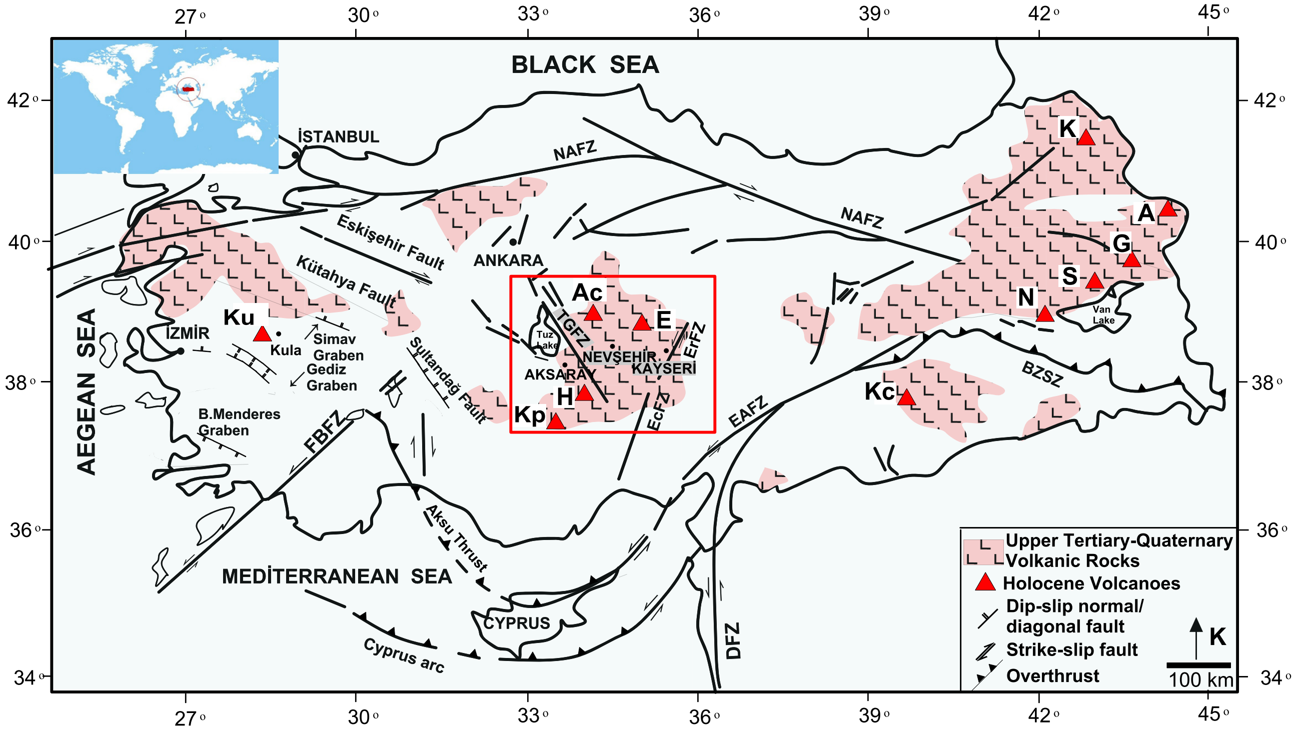

Figure 1. Upper Tertiary-Quaternary volcanic units in Turkey (Modified from Aydın *et al.* 2005). NAFZ: North Anatolian Fault Zone, EAFZ: East Anatolian Fault Zone, DFZ: Dead Sea Fault Zone, FBFZ: Fethiye Burdur Fault Zone, BZSZ: Bitlis Zagros Suture Zone, EPF: Ezinepazarı Fault, TGF: Tuz Gölü Fault; EcF: Ecemiş Fault, ErF: Erciyes Fault, DF: Deliler Fault, A: Ağrı Mountain, Ac: Acıgöl, E: Erciyes Mountain, G: Girekol Hill, H: Hasan Mountain, K: Kars Platosu, Kc: Karacadağ, Kp: Karapınar Volcanic Area, Ku: Kula Plateau, N: Nemrut Mountain, S: Süphan Mountain, NKM: Niğde –Kırşehir Massive. Red square shows the study area.

3.2 Determination of palaeodirection

Standard palaeomagnetic analyses comprising thermal (TH) and alternating field (AF) demagnetization of the natural remanent magnetization (NRM), were performed to determine the palaeodirections of all samples. Measurements were taken using a JR6 Spinner Magnetometer. An MMTD80 furnace and an LDA-3A degausser were used for thermal and alternating field demagnetization, respectively. 35 samples were thermally demagnetized in fourteen steps from room temperature up to 600 °C, whereas AF demagnetization was applied to 83 samples from 0 to 100 mT. The remanence vector components were defined by principal component analysis (PCA, Kirschvink 1980), and the average characteristic remanent magnetization (ChRM) was calculated using the Fisher (1953) statistical analysis. All demagnetization data were analyzed using RemaSoft 3.0 (Chadima & Hrouda 2006). To understand the evolution of the palaeogeography of the study area in the last 5 Ma (upper Miocene to present), the pole position was calculated using the mean palaeomagnetic directions obtained from 12 sites with reliable results in these studies. It was then compared to the pole position in Stable Europe with an age of 5 Ma (Besse & Courtillot 2002). Then the amount of rotation (R) and transport towards the poles (T) between the observed and the reference poles was calculated.

3.3 Rock magnetic measurements

Rock magnetic investigations, comprising thermomagnetic measurements, determination of hysteresis data, isothermal remanent magnetization (IRM) acquisition experiments, Lowrie test (Lowrie 1990) and thermal demagnetization of a three-axis IRM (Lowrie 1990) were performed on selected samples to test the reliability of palaeomagnetic directions and palaeointensity data. For thermomagnetic measurements, the magnetic susceptibility of the samples was measured from room temperature to 600 °C with an MS2WF oven mounted on a Bartington magnetic susceptibility metre system. In order to examine the mineralogy, an IRM acquisition experiment and Lowrie three-axis tests (Lowrie 1990) were performed on some samples after AF demagnetized the NRM. For IRM acquisition, fields of up to 1.0 T were applied along the Z-axis (hard component) using a Molspin pulse magnetizer. By further applying different fields in three perpendicular directions (X, Y, Z) to the samples, 0.4 T (medium component) was applied to the Y-axis and 0.12 T (soft component) to the X-axis and subsequently demagnetization was applied thermally and the magnetic mineral carriers were identified based on their coercive and unblocking behaviour. Hysteresis parameters of pilot samples were obtained by using a 4″ Princeton Measurements Corporation Alternating Gradient magnetometer (MicroMag).

3.4 Microscope analysis

Five selected polished thin sections were analysed with an optical microscope under reflected light in oil immersion and a polarized light microscope to characterize opaque minerals (i.e. mainly magnetite/titanomagnetites).

3.5 Palaeointensity determination

Palaeointensity determinations were carried out using the modified form (Coe *et al.* 1978) of the Thellier & Thellier (1959) method. The stepwise double heating method including pTRM check applied the

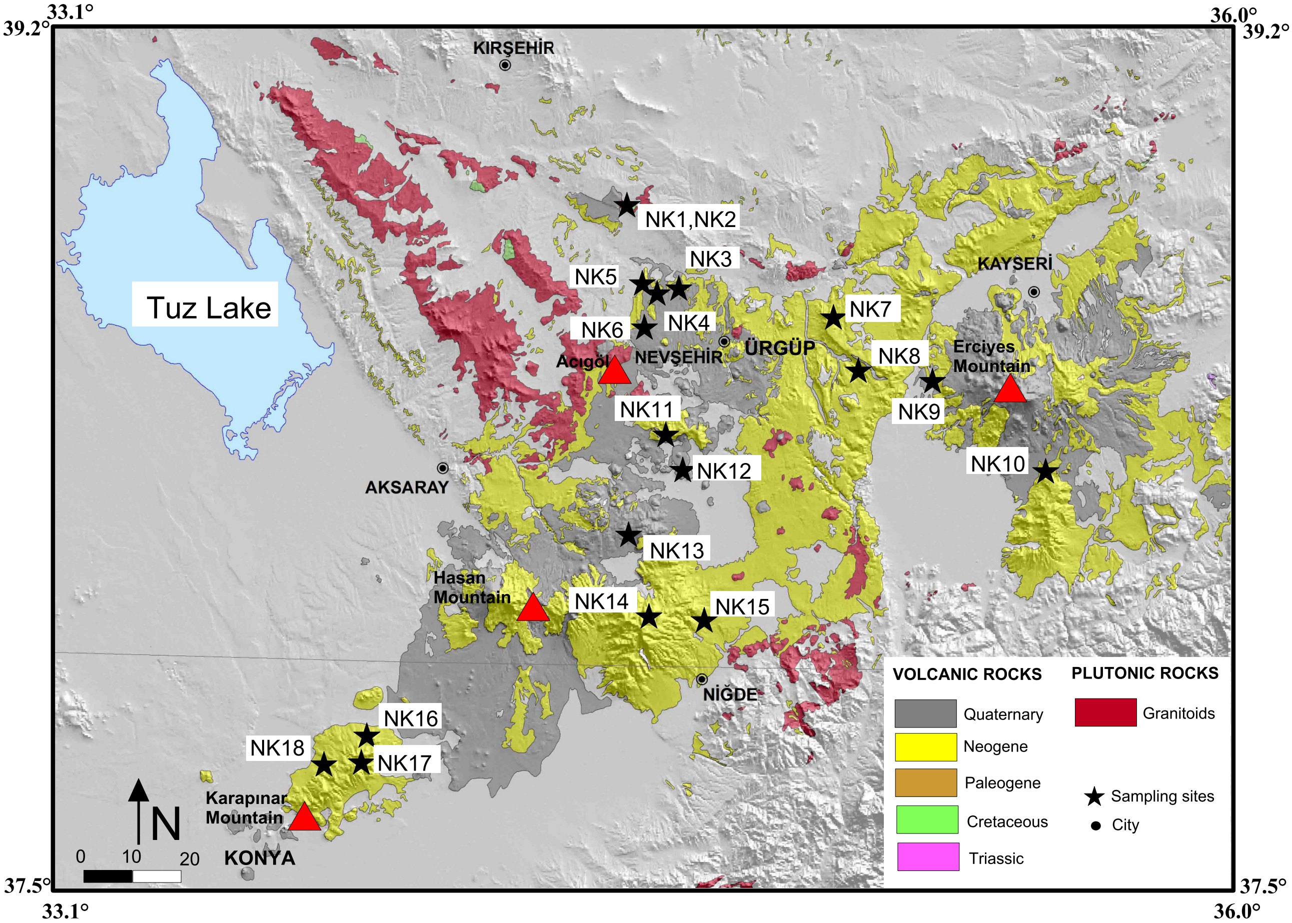

Figure 2. Geological map of study area (red square in Fig. 1). Sampling sites (black stars) and distribution of the Quaternary and Neogene volcanic mountains (red triangles) in Central Anatolia (Modified from MTA 2013).

Table 1. Coordinates and ages of studied sites: (1) Platzman *et al.* (1998), (2) Doğan (2011), (3) Aydar *et al.* (2013) and (4) Mues-Schumacher & Schumacher 1996.

Site	Coordinates	Age (Ma)	Method	Reference
Quaternary volcanic unit				
NK1	38° 52.183′N/34° 27.432′E	1.28 ± 0.038	Ar-Ar	(2)
NK2	38° 52.183′N/34° 27.432′E	1.28 ± 0.038	Ar-Ar	(2)
NK3	38° 45.161′N/34° 36.637′E	0.08 ± 0.03	K/Ar	(1)
NK4	38° 45.742′N/34° 32.637′E	0.096 ± 0.013	Ar-Ar	(2)
NK5	38° 46.368′N/34° 30.575′E	1.98 ± 0.040	Ar-Ar	(2)
NK6	38° 40.604′N/34° 30.488′E	0.71 ± 0.03	K/Ar	This study
NK8	38° 34.107′N/35° 4.359′E	1.1 ± 0.1	K/Ar	(4)
NK9	38° 33.771′N/35° 11.741′E	1.84 ± 0.47	K/Ar	(1)
NK10	38° 21.525′N/35° 29.005′E	2.16 ± 0.58	K/Ar	(1)
NK11	38° 26.122′N/34° 35.108′E	2.15 ± 0.93	K/Ar	(1)
NK12	38° 21.946′N/34° 38.741′E	<0.2	K/Ar	(1)
NK13	38° 13.241′N/34° 26.293′E	1.48 ± 0.5	K/Ar	(1)
NK14	38° 5.194′N/34° 25.588′E	2.57 ± 1.5	K/Ar	(1)
NK16	37° 51.015′N/33° 51.952′E	2.32 ± 0.51	K/Ar	(1)
Neogene volcanic unit				
NK7	38° 38.812′N/34° 58.252′E	8.26 ± 0.16	Ar-Ar	(3)
NK15	38° 2.379′N/34° 38.856′E	4.43 ± 1.6	K/Ar	(1)
NK17	37° 48.098′N/33° 51.896′E	5.98 ± 0.25	K/Ar	(1)
NK18	37° 47.590′N/33° 45.213′E	4.7 ± 0.2	K/Ar	(1)

Table 2. K-Ar geochronology results. The uncertainty of the age calculated falls within 2σ error.

Sample	K, per cent $\pm\ \sigma$	40Ar rad (ng g^{-1})	Per cent 40Ar air	Age (Ma)	Error 2σ
NK6	1.99 ± 0.02	0.0976 ± 0.016	84.2	0.710	0.030

laboratory field of 35 μT with a field accuracy of 0.1 μT during heating and cooling. Palaeointensity determinations for all samples were performed using an MMTD80 thermal demagnetizer with all heating-cooling runs performed in air, and remanence was measured with a JR6 Spinner Magnetometer.

Palaeointensity determinations were performed according to the MT4 protocol (Leonhardt *et al.* 2004a), which applies modified Thellier & Thellier (1959) methods. The MT4 protocol also includes additivity checks (Krása *et al.* 2003), pTRM (partial thermoremanence) check (Coe 1967) and pTRM tail checks (Riisager & Riisager 2001). The pTRM refers to partial thermoremanence acquired during a heating/cooling cycle from room temperature to the chosen heating temperature. Repeated demagnetization to Ti, which is the temperature step after previous pTRM acquisition to Ti or so-called pTRM-tail check, tests the independence of different pTRMs (Riisager & Riisager 2001; Leonhardt *et al.* 2004b). The additivity check detects violations of the law of additivity for pTRMs (Krása *et al.* 2003). This check is essentially the same as the zero-field alteration check. However, when conducting in-field plus zero-field checks, comparing both values indicates possible failures of Thellier's law of additivity (Leonhardt *et al.* 2004b). The original Thellier method (Thellier & Thellier 1959) includes many heating steps, potentially causing the alteration of minerals responsible for magnetization. For this reason, additional controls are required to obtain a reliable result from the measurements (Selkin & Tauxe 2000; Kissel & Laj 2004; Leonhardt *et al.* 2004a; Dunlop 2011; Paterson *et al.* 2014, b; Tauxe & Staudigel 2004; Yu & Tauxe 2005; Shaar & Tauxe 2013). Samples were subjected to 15 double heating-cooling runs up to 600 °C and 7 pTRM-checks were performed after heating the samples to 100, 250, 340, 400, 460, 510 and 550 °C. pTRM-tail and additivity checks were performed in three steps from 200, 400 and 550 °C and 250, 400 and 510 °C, respectively.

Most of these criteria are based on Arai plots (Nagata *et al.* 1963), focusing on the arrangement of data points along a straight line (e.g. Coe *et al.* 1978; Yu & Tauxe 2005) and effects of thermal alteration on partial TRMs (Selkin & Tauxe 2000; Leonhardt *et al.* 2004b). All palaeointensity determinations were analysed using the Thellier Tool 4.22 software (Leonhardt *et al.* 2004a), which includes the determination of classes A and B based on selection acceptance criteria by Leonhardt *et al.* (2004a) and Paterson *et al.* (2014). All criteria and thresholds used in this study are shown in Table 4. This software allows full vector analysis and the application of a check correction (Valet *et al.* 1996; Leonhardt *et al.* 2003). The reliability of the data decreases because of the domain structures of the samples, high degree of alteration and changes in magnetic mineralogy during heating and cooling throughout the measurements (Leonhardt *et al.* 2003, 2004b). The pTRM check, used for correcting the palaeointensity determination, is sensible for alteration below the temperature at which the check is performed. Therefore, the alteration product, which forms during thermal demagnetization, must only affect unblocking temperatures below the subsequent alteration. The pTRM checks help identify the mechanisms of alteration. This corrected alteration check is then only reasonable for magnetomineralogical changes and could be used for alteration correction methods (e.g. Valet *et al.* 1996) even if MD particles are present (Leonhardt *et al.* 2003, 2004b). For this reason, attempts were made to apply the check correction (Valet *et al.* 1996), and then the most reliable samples (Leonhardt *et al.* 2004a) could be identified. After applying the check correction, the additivity checks should fall on the corrected pTRM values for cases of SD remanence because the fundamental prerequisite for this correction method is the absence of MD remanence (Leonhardt *et al.* 2003). Here, the check correction was applied for samples that did not pass the acceptance criteria. After this correction, the classes are described as A* and B* and accepted as reliable (Fig. 10c).

4 RESULTS

4.1 Determination of palaeodirection

Palaeomagnetic directions are listed in Table 3. The maximum unblocking temperatures of most samples lie around 580–600 °C suggesting the presence of low-Ti titanomagnetite (Figs 3a and c). Figs 3(b) and (d) show the directional variation of two selected samples during AF demagnetization. A small viscous remanent magnetization component was removed at 5 mT AF peak amplitude. It appears that almost all samples carry two component palaeomagnetic directions demagnetized between 5–30 and 30–100 mT, respectively, with vector endpoints finally migrating towards the origin (Figs 3b and d). Low α_{95} values for almost all sites indicate stable palaeomagnetic directions, except for two sites (NK1 and NK2), where α_{95} angles range from 18.3° to 24.9° (Table 3).

Since the palaeohorizontal of the volcanic rocks used in the study is zero, the fold test was not applied. However, 3 of the 12 sites used in palaeointensity calculations for the Pleistocene–Miocene interval have reversed polarity (Fig. 4a). Therefore, a reversal test (Tauxe *et al.* 1991) was applied. First, the reversed polarity mode was converted to its antipode, and then the bootstrap test was applied separately to the other polarity. It was shown that the 95 per cent confidence intervals (red and blue lines) for normal polarity and reverse antipodes of the mean X, Y, and Z components in Cartesian coordinates overlap (Fig. 4b). Therefore, the data from this site pass the bootstrap reversal test.

The rotation amount was calculated as $R+\Delta R = 13.1° \pm 7.3°$ and the transport amount towards the poles as $T\pm\Delta T = 6.4° \pm 6.4°$. According to these results, the study area rotated by 13.1° counterclockwise relative to the Stable European Pole Position from the upper Miocene to the present. This rotation amount in the study location is not local, and it is to be related to the consequences of rotation during the westward escape of the Anatolian Block. This counter-clockwise rotation amount was also confirmed by modern GPS data (Reilinger *et al*. 1997).

4.2 Magnetic mineralogy

The thermomagnetic results are presented in Fig. 5, with 25 per cent of the samples exhibiting a considerable difference between heating and cooling curves, such as in Figs 5(a) and (b), due to alteration. Samples were characterized by a dominant phase of low to rich-Ti magnetite with a small fraction of hematite (e.g. NK6, NK8)

Table 3. Palaeomagnetic directions. *N*/*n* denotes the number of sites used for site mean calculation. Declination (*D*) and inclination (*I*) describe the mean directions in geographic coordinates, respectively. α_{95} is the 95 per cent confidence circle and *k* is the precision parameter (Fisher 1953). *R* is the resultant vector. ΔDX and ΔIX are the declination and inclination errors calculated after Deenen *et al.* (2011).

Site	*N*/*n*	*D*	*I*	ΔDx	ΔIx	*R*	*k*	α_{95}
Pleistocene								
NK1	6/6	149.5	− 52.7	30.0	26.0	5.6	14.3	18.3
NK2	7/5	206	− 50	30.0	28.4	4.6	11.2	24.9
NK3	14/14	354.5	34.5	5.0	7.2	13.8	58.8	5.2
NK4	12/12	355.8	36.1	7.7	10.7	11.7	33.0	7.7
NK5	8/7	10.6	65.0	8.7	4.6	7.0	192.8	4.4
NK6	11/11	351.7	47.7	7.4	7.7	10.8	52.5	6.4
NK8	11/11	167.5	− 41.5	5.6	6.9	10.8	70.3	5.5
NK9	8/6	131.7	− 53.6	11.1	9.4	5.9	96.4	6.9
NK10	10/9	236.8	− 5.1	9.9	19.6	8.7	25.5	10.4
NK11	7/7	161.2	− 33.6	6.7	9.8	6.9	50.0	8.7
NK12	6/4	352.1	56.1	9.8	7.5	4.0	408.8	4.5
NK13	7/7	208.6	− 63.4	16.3	9.2	6.7	25.8	12.1
NK14	1212	164.5	− 53.2	5.7	5.0	11.9	88.8	4.6
Pliocene								
NK15	8/8	358.9	54.4	10.5	8.7	7.9	63.1	7.0
NK16	5/4	178.7	− 58.4	12.3	10.8	4.0	115.2	8.6
NK18	6/6	7.4	42.9	6.7	7.9	6.0	129.9	5.9
Miocene								
NK7	5/5	213.6	− 67.6	20.0	9.0	4.9	84.3	8.4
NK17	10/10	154.4	− 43.4	5.6	6.5	9.9	91.4	5.1

Table 4. Criteria used in classification of palaeointensity (Leonhardt *et al.* 2004a and Paterson *et al.* 2014).

Class A	Class B
Linear fit criteria	
Number of points ≥ 5	Number of points ≥ 5
Standard deviation ≥ 0.1	Standard deviation ≥ 0.15
Fraction of NRM:(f) ≥0.5	Fraction of NRM:(f) ≥0.3
Quality factor (q) ≥5	Quality factor (q) ≥2
Directional criteria	
MAD (anchored) ≤6	MAD (anchored) ≤15
Alpha ≤ 15	Alpha ≤ 15
Alteration criteria	
Relative check error:(d(CK)) ≤5	Relative check error: (d(CK)) ≤7
Cumulative check diff : (d(pal)) ≤5	Cumulative check diff : (d(pal)) ≤10
Repeated demagnetazition steps	
Normalized tail of PTRM: d (t*) ≤3	Normalized tail of PTRM: d (t*) ≤99
Relative intensity diff : d(TR) ≤10	Relative intensity diff : d(TR) ≤15
Addivity checks	
Relative AC error: (d(AC)) ≤5	Relative AC error: (d(AC)) ≤10

and maghemite (e.g. NK7, NK14). The heating curves of samples from Figs 5(a) to (e) characteristically showed Fe–TiO minerals rich in Ti. In samples from NK16 and NK17, heating and cooling curves mostly coincided, showing the thermal characteristics of pure magnetite (Figs 5r and s). Some of the samples also had a tiny high-temperature phase which was removed at about 620 °C, indicating hematite (e.g. NK6, NK8). A comparison of thermomagnetic and palaeointensity results clearly shows that whereas reliable palaeointensity values were obtained for samples such as NK18, NK8 and NK17 samples with low alteration, reliable palaeointensity data could not be obtained for the highly altered NK1 and NK2 samples.

In samples examined under polarized light, opaque minerals were observed. There was no alteration, the main mineral was mostly plagioclase, and also pyroxene, biotite and quartz minerals were found (Figs 9a, e, i, c, g and k). Reflected light microscopy of samples showed that magnetite was the main magnetic mineral (Figs 9b, f, j, d, h and l). Some magnetites were transformed into hematite (NK8b), indicated by red internal reflections along the marginal zones, and transformed into ilmenite (NK8a). Sample NK18 contains oxidized magnetic minerals characterized by magnetite–hematite, magnetite–maghemiteand magnetite–lmenite (Fig. 9). Microscopy analysis indicated the primary igneous texture for selected samples. Together the thermomagnetic and microscopy

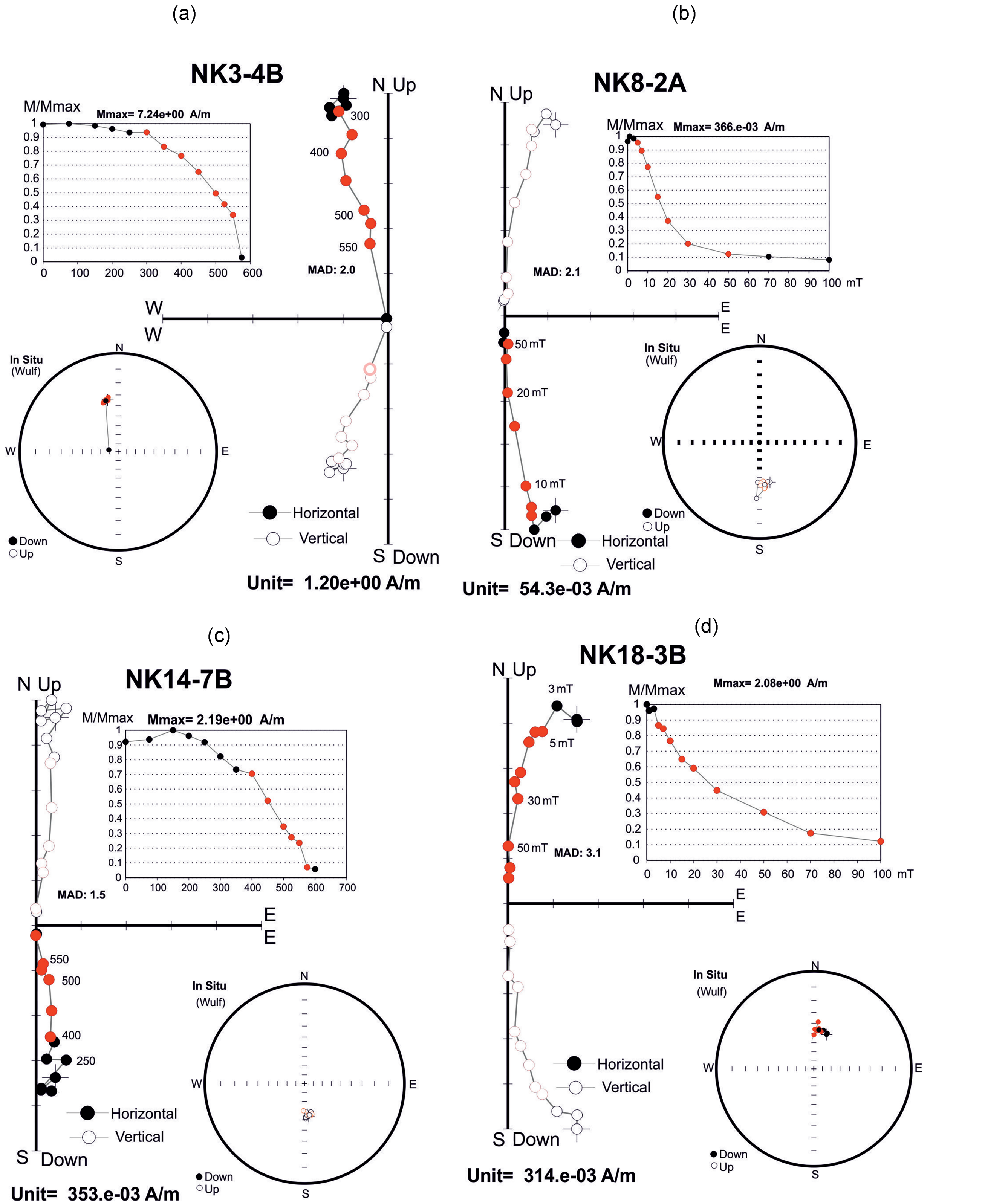

Figure 3. AF and thermal demagnetization results from selected samples, displayed as Zijderveld diagrams, stereonet, normalized intensity. MAD (maximum angular deviation). Red dots show the ChRM directions obtained from data using PCA analysis.

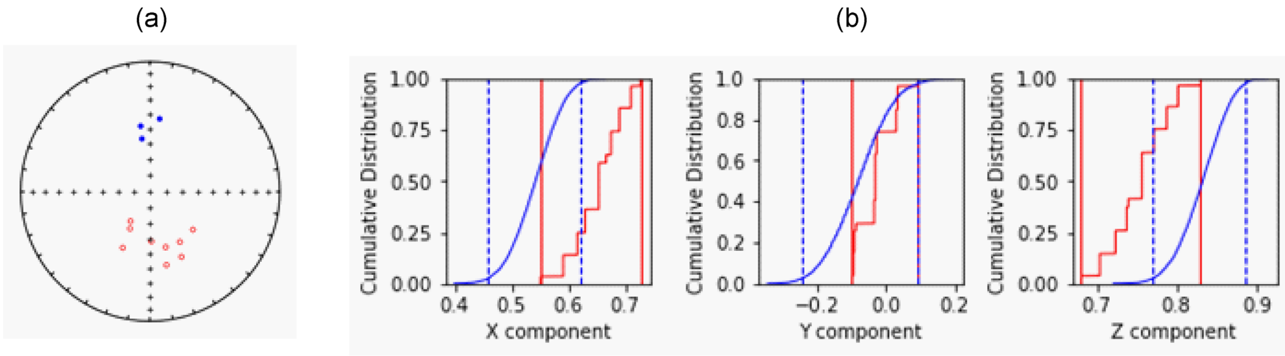

Figure 4. A bootstrap test for common mean (Tauxe *et al.* 1991). (a) Equal-area projection of directional data from this study (in stratigraphic coordinates). Solid symbols: lower hemisphere; open symbols: upper hemisphere. (b) Cumulative distributions of the Cartesian coordinates of the means of the bootstrapped directions from 1000 pseudosamples. The confidence intervals (vertical lines) for the data sets overlap for *X*, *Y* and *Z*, confirming that the two means cannot be distinguished at the 95 per cent confidence level.

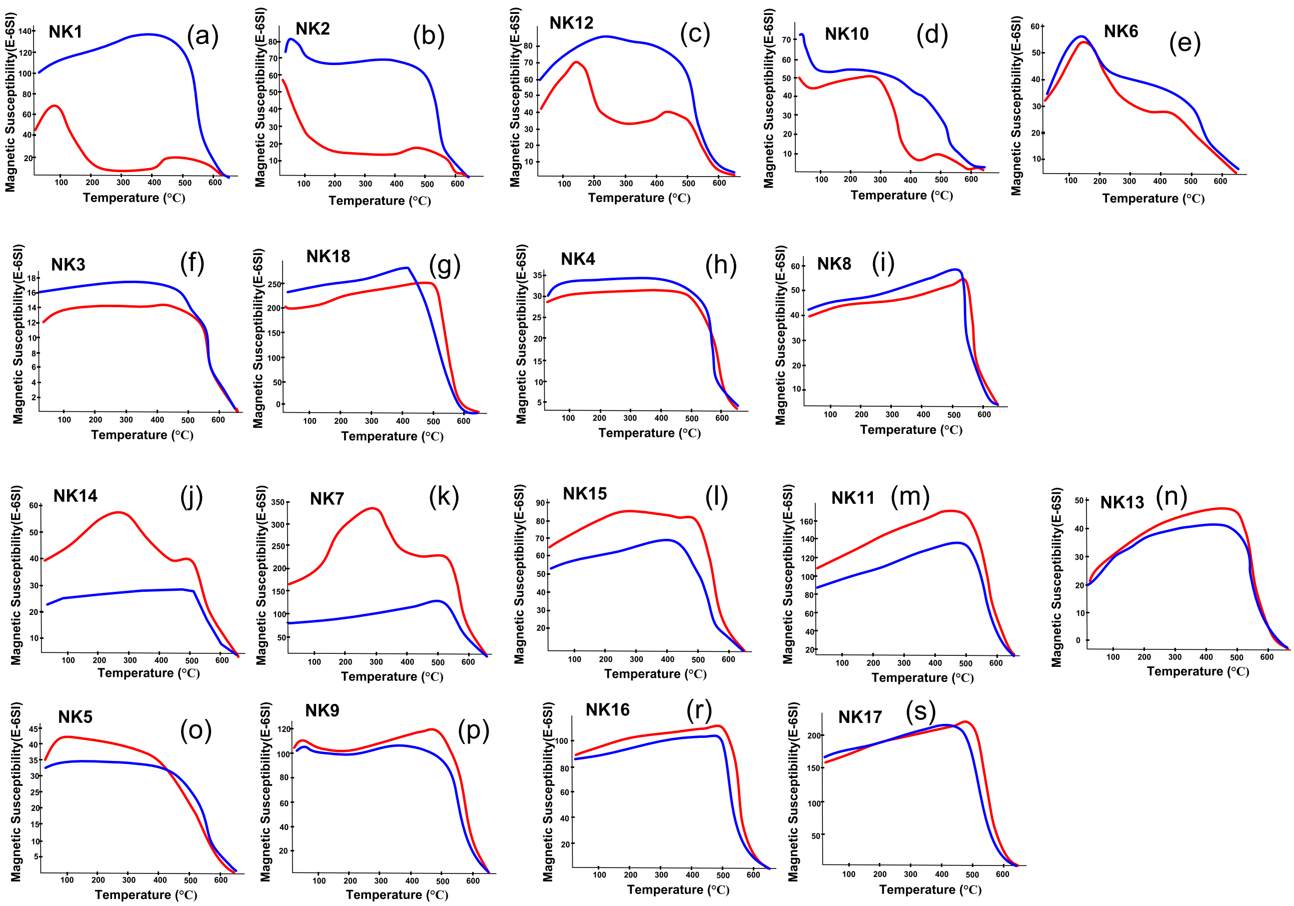

Figure 5. Thermomagnetic analysis of a selected sample from each of the studied sites. Red and blue lines indicate heating and cooling curves, respectively.

results confirm that Ti-poor magnetite is the primary magnetic carrier, along with a small fraction of maghemite and hematite (Figs 5 and 9).

IRM acquisition curves show two types (Type 1 and Type 2) of behaviour. While the Type 1 magnetization (NK1, NK2, NK5 and NK10) reaches saturation at 300 mT, Type 2 found in the samples from two sites (NK7 and NK16) nearly reached saturation at ∼600 mT, indicating the presence of a somewhat magnetically more complex phase than Type 1 (Fig. 7). According to Lowrie tests, all samples dominantly contained a low-coercivity (0.12 T) magnetic phase with maximum unblocking temperature between 400 and 580 °C, proving that the minerals responsible for magnetization are (titano) magnetites (Fig. 8). According to the hysteresis analysis results shown in Fig. 6, all samples yielded narrow hysteresis curves, which indicate low coercivity magnetic minerals (e.g. magnetite). In the Day plot (Day *et al.* 1977), most samples plotted in the pseudo-single domain area. Based on the theoretical values of Dunlop (2002), the pseudo-single domain (PSD) distribution may consist of a mixture of single-domain (SD) and multidomain (MD) grains. The samples analysed in this study contained 20–90 per cent grains of SD particles. The hysteresis experiment and Lowrie three-axis IRM tests showed that most of these samples are characterized

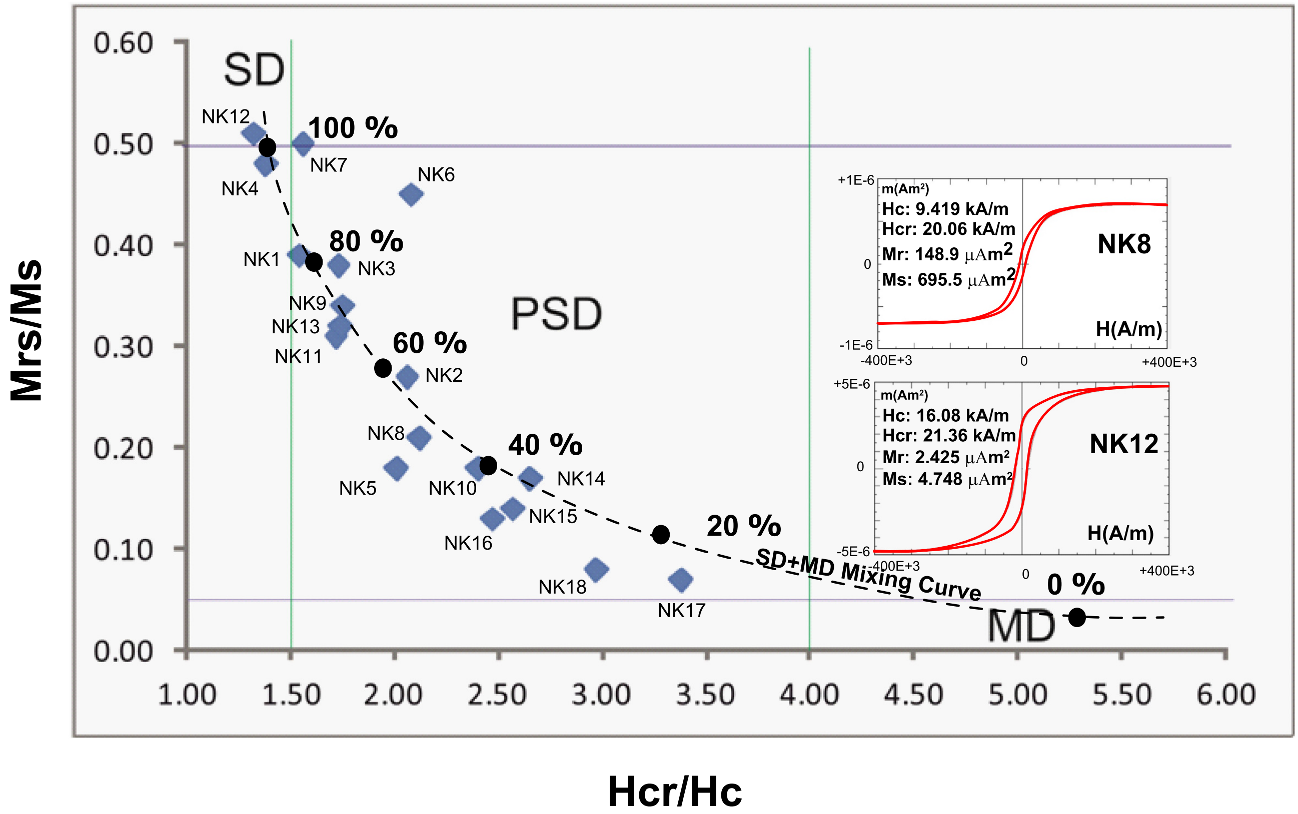

Figure 6. The hysteresis curves and Day plot diagram (Day *et al.* 1977) for representative samples. Mrs, saturation remanence magnetization; Ms, magnetic saturation; Hcr, coercivity of remanence; Hc, magnetic coercivity; SD, single domain; PSD, pseudosingle domain and MD, multidomain.

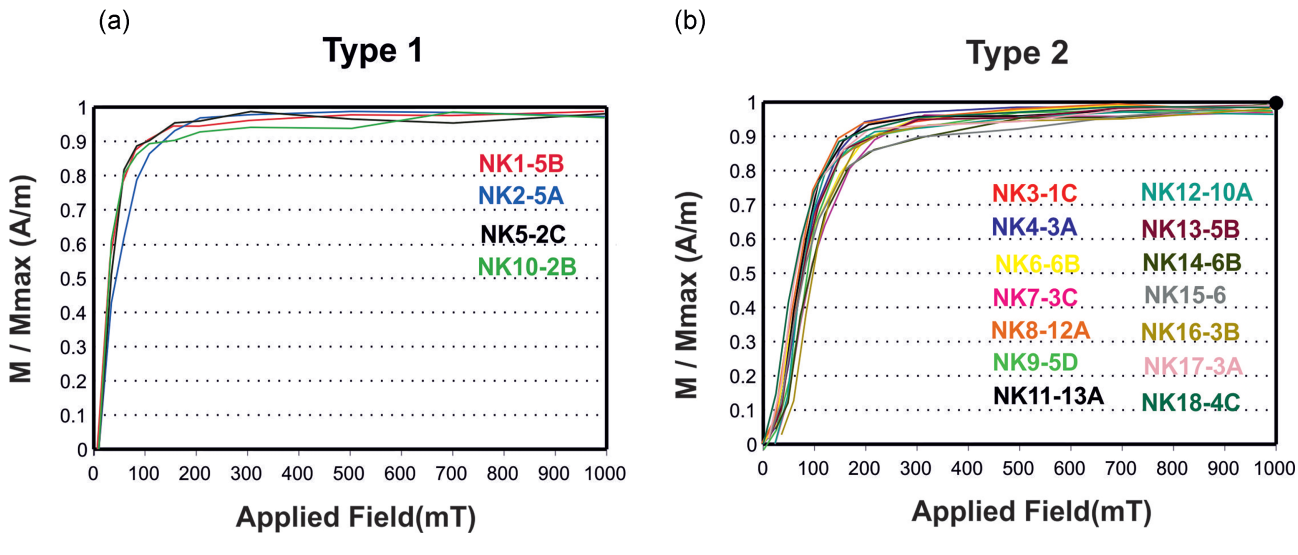

Figure 7. IRM acquisition curves for each site.

by the PSD domain state of magnetite/titanomagnetite-bearing minerals.

4.3 Palaeointensity results

Palaeointensity studies were conducted on 123 samples from eighteen sites. One hundred and five samples from 12 sites were accepted as suitable for palaeointensity determination, with 63 samples passing the reliability criteria. The check correction was applied to 42 of the samples from these 63 samples (Table 5). Analysis of palaeointensity determinations was performed using standard NRM/pTRM plots (Fig. 10). Only successive points were used to identify linear segments within NRM/pTRM diagrams. Palaeointensity results were displayed on an Arai plot (Nagata *et al.* 1963) with the absolute value of the slope of the NRM remaining plotted versus the pTRM gained (Table 5 and Fig. 10). In this study, the data in classes A and B were accepted as reliable (Figs 10a and b).

The reliable results from Pleistocene sites (NK3, NK4, NK6, NK8, NK9, NK11, NK12, NK13 and NK14) between the ages

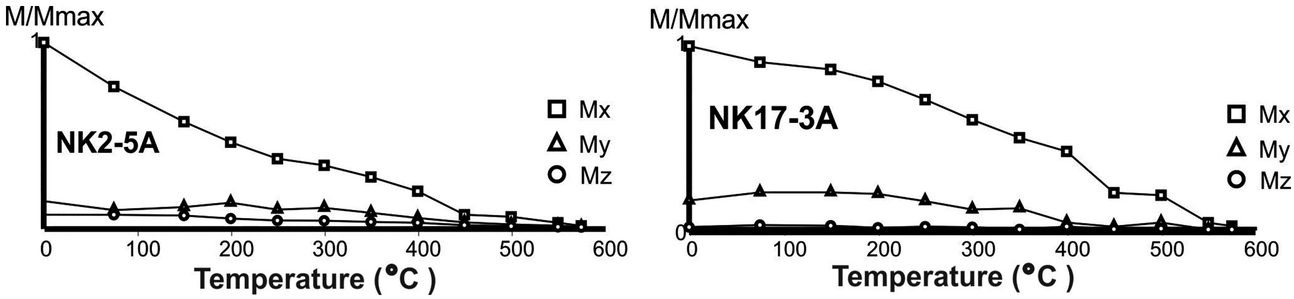

Figure 8. Thermal demagnetization of three-component IRM, followed by 1 T (hard) along the *z*-axis, 0.4 T (medium) along the y-axis, and then 0.12 T (soft) along *x*-axis T (along *z*-axis), medium (0.4 along *y*-axis) and soft (0.12 T along the sample *x*-axis).

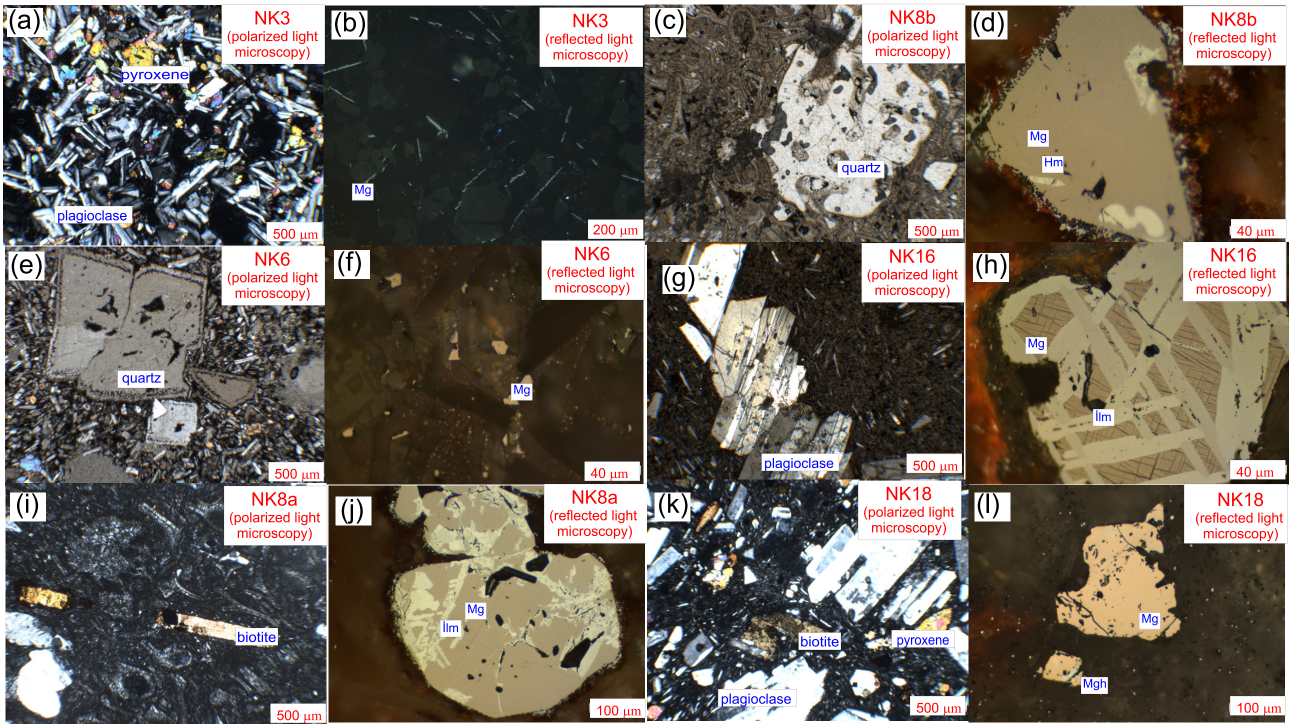

Figure 9. Representative polarized and reflected light microscope images (Mg: magnetite, Mgh: maghemite, İlm: ilmenite, Hm: hematite).

of 0.08–2.57 Ma, comprising 51 samples, were obtained by applying check correction to only 32 out of 82 samples studied. The average palaeointensity [virtual dipole moment (VDM)] values varied between 25.0 ± 7.9 μT (4.6 × 10^{22} ± 1.4 Am^2) and 79.6 ± 19.3 μT (14.8 × 10^{22} ± 3.6 Am^2; Table 5, Figs 11a and b). The average palaeointensity (VDM) values for Pleistocene sites were calculated to be 51.5 ± 16.4 μT (10.3 × 10^{22} ± 3.7 Am^2) (Table 5, Fig. 13). Reliable results obtained from Pliocene sites NK15 (age 4.43 ± 1.6 Ma) and NK18 (age 4.7 ± 0.2 Ma) include eight samples, with six samples subjected to a check correction. Palaeointensity (VDM) values of the three samples from the site NK15 show large scatter, varying between 25.2 ± 3.1 (4.6 × 10^{22} Am^2) and 91.8 ± 9.6 (16.8 × 10^{22} Am^2; Table 5). The average palaeointensity (VDM) values from sites NK15 and NK18 were calculated to be 60.0 ± 33.4 μT (10.1 × 10^{22} ± 6.1 Am^2) and 21.0 ± 4.7 μT (4.4 × 10^{22} ± 1.0 Am ^{2}), respectively (Table 5; Figs 11a, b and 12). The average palaeointensity (VDM) value calculated from site NK17 with upper Miocene age was 48.6 ± 9.2 μT (10.1 × 10^{22} ± 1.9 Am^2), which is higher than the present-day field (~47 μT/7.7 × 10^{22} Am^2; Table 5; Figs 11a and b).

5 DISCUSSION

5.1 Directional change over the Quaternary-Neogene period

The palaeomagnetic directions (*D*/*I*) from Late Pleistocene sites (NK3, NK4) were 354.5°/34.5°and 355.8°/36.1°, respectively (Table 3; Figs 11c, d and 12b). These values are also consistent with the normal polarity period of Brunhes Chron (Cande & Kent 1995). It also shows high agreement with data from a similar latitude range (Mankinen 1994; Laj *et al.* 1997). Directional (*D*/*I*) values of 352.1°/56.1°, 351.7°/47.7°, 167.5°/−41.5° and 208.6°/−63.4° obtained from sites NK12 (age <0.2 Ma), NK6 (age 0.7 Ma), NK8 (age 1.1 Ma) and NK13 (age 1.48 Ma), respectively, corresponding to the Brunhes and Matuyama Chrons (Table 3; Figs 11c, d and 12b). Directional values of sites NK9, NK11 and NK14 were found to be 131.7°/−53.6°, 161.2°/−33.6° and 164.5°/−53.2°, respectively (Table 3; Figs 11c, d and 12b). Declinations are between 120°−180° accompanied by negative inclinations. Thus, obtained directions are coherent with the Matuyama Chron of predominantly reversed polarity (Table 3; Figs 11c, d and 12b). Declination and

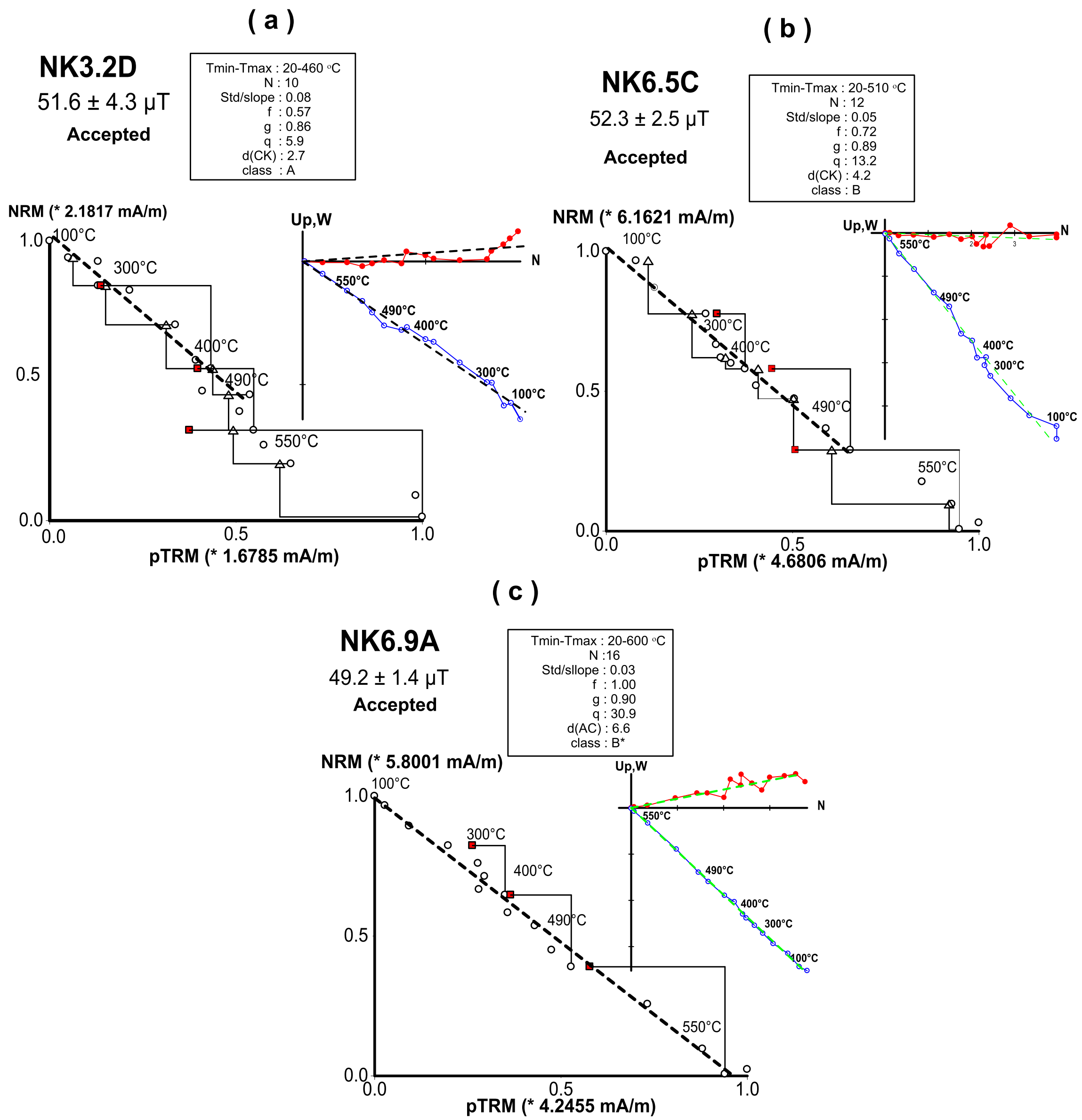

Figure 10. Arai plots. Triangles show pTRM checks; circle show a acquisition pTRM and red squares show additivity checks.

inclination of Pliocene sites NK15 and NK18 were determined as 358.9°/54.4° and 7.4°/42.9°, respectively, indicating normal polarity which could be related with subchrons in Gilbert (Table 3; Figs 11c, d and 12b). The palaeointensity (VDM) values of 20.98 ± 4.7 μT ($4.38 \times 10^{22} \pm 0.98$ Am^2), less than 50 per cent of the present-day field, from site NK 18 (age 4.7 ± 0.2 Ma), which lies in the negative polarity Gilbert Chron, were found to be lower than average values obtained from the Gilbert Chron (Doell & Dalrymple 1966), while inclinations indicate normal polarity that does not coincide with the Gilbert Chron (Table 5; Figs 11 and 12). These results coincide with a period of significant intensity drop, which could indicate the Nunivak (4.4–4.6 Ma) or Sidufjall (4.8–4.89 Ma) subchrons (Cande & Kent 1995). There are still uncertainties in the dating of the Nunivak subchron. According to the results from a few studies, the Nunivak subchron occurred at 4.4–4.6 Ma (Cande & Kent 1995) and 4.47–4.642 Ma (Lisiecki & Raymo 2005). Since the standard age deviation (Platzman *et al.* 1998) and palaeointensity values for site NK15 have a wide distribution, a clear argument for the subchrons was not made based on NK15. The palaeomagnetic direction of one site from the Miocene was 154.4°/−43.4°, indicating reversed polarity compared to the predominantly reversed Gilbert Chron (Table 3; Figs 11c, d and 12b).

The highest VDM value was obtained at 0.08 Ma with 14.7×10^{22} Am^2 (Table 5, Figs 11a and 12a), ~90 per cent higher than the axial dipole moment in 2020 with 7.7×10^{22} Am^2 (according to the 13th Generation International Geomagnetic Reference Field, IGRF-13, Wardinski *et al.* 2020). Field excursions can probably cause large-amplitude fluctuations, which are frequently present during polarity intervals. Between the pre-reversal and post-reversal periods, the first is associated with a long-term decrease and low field intensity, whereas intense and rapid recovery occurs during the second phase (Valet 2003). The presence of high magnetic field strength before excursions such as Laschamp (Valet 2003; Channell *et al.* 2009; Nowaczyk *et al.* 2013; Laj *et al.* 2014), Norwegian–Greenland Sea (NGS; Channell *et al.* 2009; Liu *et al.* 2020); Post Blake (Singer *et al.* 2014) and Iceland Basin (Channell *et al.* 2009)

Table 5. Palaeointensity results. Site: Code for the sample *n*/*N* shows successful versus attempted palaeointensity determinations. T_{min} and T_{max} specify the temperature range of the straight line segment calculated over Np successive points. **f**: The fraction used to define the chosen NRM/TRM segment, **g:** the gap factor and **q:** the quality factor were calculated according to Coe *et al.* (1978). **w** denotes the weighting factor of Prèvot *et al*. (1985). **Mad (anc):** Mean angular deviation anchored, **d(CK):** the difference between pTRM-check and related pTRM acquisition, **d(t*)**: normalized pTRM-tail d(t*) (Leonhardt *et al.* 2004a), **d(TR)**: Difference in intensity between initial and iteration demagnetization step, **d(AC)**: Difference between pTRM control and addition control, **C:** defines the class as described in the criteria section. *****Indicates that check correction was applied. **PI** is the palaeointensity values with associated standard deviation (SD) for the individual determination and the weighted site mean, respectively, **VDM**: Virtual dipole moment.

Site	Age (Ma)	n/N	Specimen	T_{min}	T_{max}	N_p	f	g	q	w	MAD	d(CK)	d(AC)	d(TR)	d(t*)	Class	PI ± SD (μT)
PLEISTOCENE																	
NK3	0.08 ± 0.03	5/9	NK3.2D	20	460	10	0.57	0.86	5.9	2.1	2.7	2.7	3.8	6.7	12.3	A	51.6 ± 4.3
			NK3.3C	20	400	8	0.39	0.81	6.2	2.5	1.6	2.3	0.9	3.4	1.5	B	59.9 ± 3.1
			NK3.4C	300	510	8	0.36	0.78	3.1	1.3	2	6.1	4.9	3	2.2	B	74.9 ± 6.8
			NK3.5C	200	460	8	0.37	0.85	3.6	1.4	2.3	4.7	5.8	4.7	12.8	B	74.6 ± 6.7
			NK3.9C	100	510	11	0.47	0.86	2.7	0.9	3.7	0	4.2	4.2	0	B*	64.6 ± 9.5
														PIw ± SD (μT)			**65.1 ± 9.9**
														Mean VDM (Am^2)			**14.7E + 22 ± 2.2E + 22**
NK4	0.096 ± 0.013	10/10	NK4.1B	340	490	6	0.34	0.68	1.7	0.9	1.4	6.5	1.8	2.2	12.7	B	68.9 ± 9.1
			NK4.1C	20	530	13	0.59	0.88	14.6	4.4	3.2	0	9.6	1	16.7	B*	60.6 ± 2.1
			NK4.2C	20	600	16	1	0.88	28.6	7.7	2.4	0	4.9	13.5	25.7	B*	39.9 ± 1.2
			NK4.3C	490	600	6	0.73	0.66	8.8	4.4	3	6.9	8.6	12.2	21	B	36.0 ± 1.9
			NK4.5A	200	550	12	0.7	0.82	6.1	2.2	2.2	0	8.7	5	10.3	B*	69.3 ± 6.5
			NK4.7B	510	600	5	0.64	0.57	3.5	2	1.1	0	10	9.4	19.6	B*	30.1 ± 3.2
			NK4.8B	100	510	11	0.42	0.86	2.7	0.9	2.4	0	6.9	1.7	12.7	B*	86.9 ± 11.6
			NK4.9A	340	600	11	0.94	0.79	5.9	2	2.5	6.1	7.5	14.3	28.3	B	44.1 ± 5.5
			NK4.10A	200	600	14	0.97	0.86	8.2	2.4	2.4	4.8	6.5	4.4	8.5	B	56.3 ± 5.7
			NK4.11A	200	510	10	0.4	0.84	2.5	0.9	2.2	3.4	2.8	3.2	22.5	B	66.1 ± 8.7
														PIw ± SD (μT)			**55.9 ± 17.8**
														Mean VDM (Am^2)			**12.4E + 22 ± 3.9E + 22**
NK6	0.710 ± 0.03	8/10	NK6.1B	20	370	7	0.32	0.76	7	3.1	2.2	4.2	8	2.2	8.6	B	51.2 ± 1.8
			NK6.3	20	510	12	0.52	0.83	3.8	1.2	2.6	0	8.3	7.2	13.2	B*	63.7 ± 7.2
			NK6.5C	20	510	12	0.72	0.89	13.2	4.2	2.7	4.2	8.1	4.8	10	B	52.3 ± 2.5
			NK6.5D	20	400	8	0.42	0.77	5.8	2.4	2.1	3	5.5	3.5	6.5	B	49.8 ± 2.8
			NK6.6D	20	600	16	1	0.91	14.4	3.9	2.5	0	6.2	5.1	9.1	B*	42.2 ± 2.7
			NK6.7B	20	460	10	0.64	0.83	7.7	2.7	1.2	5.7	4.8	7	12.7	B	50.7 ± 3.5
			NK6.8A	20	400	8	0.4	0.79	3	1.2	2.2	4.8	6.3	5.7	17.4	B	51.8 ± 5.4
			NK6.9A	20	600	16	1	0.9	30.9	8.3	2	0	6.6	2.1	4.9	B*	49.2 ± 1.4
														PIw ± SD (μT)			**51.3 ± 5.9**
														Mean VDM (Am^2)			**10.2E + 22 ± 1.2E + 22**
NK8	1.1 ± 0.1	6/8	NK8.1A	100	570	14	0.81	0.84	6.2	1.8	2.5	3.3	1.3	7.2	4.9	B	25.0 ± 2.7
			NK8.2B	20	570	15	0.83	0.83	7.8	2.2	4.5	4.6	5.2	8	5.4	B	25.1 ± 2.2
			NK8.2C	20	510	12	0.49	0.82	3.7	1.2	2.6	7	7.6	1.9	2.8	B	45.4 ± 5.0
			NK8.4B	20	570	15	0.85	0.81	6.2	1.7	2.2	6.7	5.8	4	2.7	B	25.4 ± 2.8
			NK8.5B	20	510	12	0.51	0.88	5.2	1.6	2.3	4.8	8.4	1.3	2.1	B	44.7 ± 3.5
			NK8.9C	20	490	10	0.31	0.86	2.9	1	3.1	0	6.1	2	1	B*	31.6 ± 2.9
														PIw ± SD (μT)			**32.8 ± 9.7**
														Mean VDM (Am^2)			**6.9E + 22 ± 2.1E + 22**

Table 5. Continued

Site	Age (Ma)	n/N	Specimen	T_{min}	T_{max}	N_p	f	g	q	w	MAD	d(CK)	d(AC)	d(TR)	d(t*)	Class	PI ± SD (μT)
NK12	<0.2	7/8	NK12.1A	20	600	16	1	0.85	16.2	4.3	2.9	0	8.7	8.3	5.3	B*	40.4 ± 2.1
			NK12.1B	20	510	12	0.67	0.83	4	1.3	4.8	0	4.3	2.2	4.5	B*	45.0 ± 6.2
			NK12.3A	20	510	12	0.69	0.82	6.2	2	3.8	0	2.7	3.6	5.4	B*	43.8 ± 4.0
			NK12.4A	20	400	8	0.51	0.75	4.7	1.9	4.1	0	5.9	4	7	B*	48.8 ± 4.0
			NK12.4B	20	510	12	0.65	0.83	3.8	1.2	3	0	6.9	3.5	3.8	B*	47.7 ± 6.8
			NK12.4C	20	510	12	0.69	0.82	6.2	2	3.2	0	1	1.5	7.5	B*	46.7 ± 4.3
			NK12.9B	20	600	16	1	0.86	11.2	3	5.3	0	3.7	4.5	5.9	B*	43.4 ± 3.4
														PIw ± SD (μT)			**45.1 ± 2.9**
														Mean VDM (Am^2)			**8.1E + 22 ± 0.5E + 22**
NK13	1.48 ± 0.5	2/11	NK13.2A	20	600	16	1	0.87	6.7	1.8	4.8	0	7.1	3.1	0.5	B*	**26.1 ± 3.4**
			NK13.3B	20	550	13	0.67	0.8	3.6	1.1	2.8	0	9.2	7	1.6	B*	**72.3 ± 10.7**
														PIw ± SD (μT)			**49.2 ± 32.6**
														Mean VDM (Am^2)			**8.0E + 22 ± 5.3E + 22**
NK9	1.84 ± 0.47	4/7	NK9.3C	300	600	12	0.93	0.86	6	1.8	2.6	0	9.1	4.4	4.2	B*	34.1 ± 4.5
			NK9.8B	100	460	9	0.3	0.76	1.6	0.6	5	0	7.2	5.5	3.6	B*	20.4 ± 2.9
			NK9.9C	20	510	12	0.61	0.88	5	1.6	4.8	0	10	1.5	1.1	B*	20.4 ± 2.2
			NK9.10C*	340	510	7	0.52	0.75	3.5	1.6	2.8	0	6.1	1.4	2.4	B*	89.8 ± 9.9
														PIw ± SD (μT)			**25.0 ± 7.9**
														Mean VDM (Am^2)			**4.6E + 22 ± 1.4E + 22**
NK11	2.15 ± 0.93	2/11	NK11.13B	370	600	10	0.89	0.83	15	5.3	4	0	6.6	7.5	17.4	B*	**53.8 ± 2.6**
			NK11.13C	510	600	5	0.55	0.64	2.7	1.5	2.8	0	6.2	5	6.5	B*	**65.5 ± 8.4**
														PIw ± SD (μT)			**59.7 ± 8.2**
														Mean VDM (Am^2)			**13.5E + 22 ± 1.8E + 22**
NK14	2.57 ± 1.5	7/8	NK14.1B	100	490	10	0.38	0.79	2.3	0.8	1.9	0	9.9	6.8	0	B*	82.1 ± 10.8
			NK14.2A	300	490	7	0.5	0.8	7.2	3.2	1.4	0	6.5	2.9	14.6	B*	104.3 ± 5.8
			NK4.4A	250	490	8	0.49	0.8	5.2	2.1	1.3	0	9.6	2	0	B*	102.6 ± 7.7
			NK14.4B	100	490	10	0.46	0.79	3.9	1.4	2.7	0	4.5	3.8	37.3	B*	82.1 ± 7.5
			NK14.7A	200	490	9	0.43	0.83	3.9	1.4	1.8	0	6.5	8.1	29	B*	66.7 ± 6.1
			NK14.8B	510	600	5	0.37	0.69	3.9	2.3	1.2	0	10	4.8	0	B*	68.0 ± 4.4
			NK14.9B	510	600	5	0.37	0.69	3	1.7	2.2	0	4.1	8	0	B*	51.3 ± 4.3
														PIw ± SD (μT)			**79.6 ± 19.3**
														Mean VDM (Am^2)			**14.8E + 22 ± 3.6E + 22**
											PLEISTOCENE Mean VDM (Am^2)						**10.3E + 22 ± 3.7E + 22**
PLIOCENE																	
NK15	4.43 ± 1.6	3/7	NK15.2	100	600	15	1	0.89	7.2	2	4.2	0	9.9	3.7	4.9	B*	**25.2 ± 3.1**
			NK15.5	20	340	6	0.35	0.79	3.9	2	1.6	3.6	7.1	4.2	1.7	B	**63.1 ± 4.5**
			NK15.10	20	340	6	0.52	0.79	3.9	2	3.8	4.7	9.9	1.2	3.9	B	**91.8 ± 9.6**
														PIw ± SD (μT)			**60.0 ± 33.4**
														Mean VDM (Am^2)			**10.1E + 22 ± 6.1E + 22**
NK18	4.7 ± 0.2	5/10	NK18.2C*	250	510	9	0.67	0.84	12	4.5	5	0	7.7	9.9	9.8	B*	46.7 ± 2.2
			NK18.3A	340	600	11	0.73	0.82	5.7	1.9	4.9	0	10	8.7	6.7	B*	26.0 ± 2.7
			NK18.4A	460	600	7	0.61	0.69	3.8	1.7	7.7	0	9.8	12	8.3	B*	16.5 ± 1.8
			NK18.4B	20	600	16	1	0.85	11	3	6.2	0	6.9	4.1	3.7	B*	24.0 ± 1.8
			NK18.6C	20	600	16	0.97	0.85	10.3	2.8	7.5	0	8.9	7.3	5.4	B*	17.4 ± 1.4
														PIw ± SD (μT)			**21.0 ± 4.7**
														Mean VDM (Am^2)			**4.4E + 22 ± 1.0E + 22**

Table 5. Continued

Site	Age (Ma)	n/N	Specimen	T_{min}	T_{max}	N_p	f	g	q	w	MAD	d(CK)	d(AC)	d(TR)	d(t*)	Class	PI ± SD (μT)
MIOCENE																	
NK17	5.98 ± 0.25	4/7	NK17.2A	370	600	10	0.63	0.81	6		2.7	0	6.6	5.1	3	B*	49.3 ± 4.2
			NK17.2B	300	600	12	0.81	0.87	7.6		2.4	0	3.8	8.6	1.4	A*	57.0 ± 5.2
			NK17.6A	370	600	10	0.72	0.82	11.6		2.7	0	7.6	5.7	3.8	B*	35.5 ± 1.8
			NK17.8	400	510	5	0.6	0.64	3.2		5.5	0	5.9	3.5	4.9	B*	52.6 ± 6.3
														PIw ± SD (μT)			**48.6 ± 9.2**
														Mean VDM (Am^2)			**10.1E + 22 ± 1.9E + 22**

was observed in high-resolution palaeointensity studies of marine sediments. Therefore, the high magnetic field strength found at 0.08 and 0.096 Ma could be related to high values that occurred in the pre-reversal episode, such as before the NGS excursion that occurred at 0.065 Ma (Løvlie 1989; Channell *et al.* 2009; Liu *et al.* 2020), or intense and rapid recovery occurring during the second phase of the Post Blake excursion that occurred at 0.091–0.106 Ma (Singer *et al.* 2014). These results support the view that the age of the Post Blake excursion should be younger than 0.096 ± 0.013 Ma.

5.2 Comparison with the PINT database and previous studies

The obtained results were compared with the PINT database (Bono *et al.* 2021; Fig. 11). Quality of palaeointensity (QPI; Biggin & Paterson (2014)) was selected as QPI ≥ 3. For comparisons of palaeointensity, declination and inclination, only reference data (Otake *et al.* 1993; Mankinen 1994; Laj *et al.* 1997; Calvo-Rathert *et al.* 2009; Avery *et al.* 2018; Tauxe *et al.* 2022; PINT database: Bono *et al.* 2021) around the studied latitude (37.5–38.5°N; Figs 11b–d) were considered, and data produced with T+ (Thellier with pTRM checks), as applied in this study, were chosen. Here, we discuss the palaeointensity results obtained from 63 samples from 12 sites (NK3, 4, 6, 8, 9, 11, 12, 13, 14, 15, 17 and 18) with ages between 0.08 and 5.98 Ma. These are detailed palaeointensity results for 51 samples from nine Pleistocene sites (age range 0.0117– 2.58 Ma; Table 5; Fig. 11), 8 samples from two Pliocene sites (age range 2.58–5.33 Ma) and 4 samples from one site in the Upper Miocene (Messinian, age 5.33–7.246 Ma; Table 5; Fig. 11). According to the quality of the data (Biggin & Paterson 2014), sites had between 3 and 5 of the 10 QPI criteria. During the Pleistocene, the palaeointensity data were mostly obtained from the Upper Pleistocene (Otake *et al.* 1993; Mankinen 1994; Laj *et al.* 1997; Avery *et al.* 2018; Tauxe *et al.* 2022; PINT database: Bono *et al.* 2021). Upper Pleistocene Site NK4 yielded values similar to site NK3, and both are significantly higher than data from PINT (Bono *et al.* 2021) and present data (Table 5; Figs 11a, b and 12a). The large scatter of results obtained from site NK4 caused a wide error margin (2σ error) for these samples (Platzman *et al.* 1998). The palaeointensity results for four sites (NK6, NK8, NK12 and NK13) with Chibanian—Calabriyen Pleistocene age (0.129–1.8 Ma) are consistent with previous studies (Otake *et al.* 1993; Laj *et al.* 1997; Avery *et al.* 2018; Tauxe *et al.* 2022). There is no palaeointensity data in the PINT database for the early Pleistocene and Pliocene periods at the same latitudes as the study region (Fig. 11b). Thus, five new data obtained from this study, ranging in age from 1.84 to 4.7 Ma, significantly contribute to global data archives. One palaeointensity data from an upper Miocene site (NK17) with an exact age had higher values than those obtained in a previous study by Calvo-Rathert *et al.* (2009; Fig. 11b).

5.3 Latitudinal comparison during the Pleistocene

In this study, data were compared with the filtered PINT database (Bono *et al.* 2021) to examine the dynamic variations in the dipole field with respect to latitude, PADM2M record (Ziegler *et al.* 2011) and the data obtained from similar latitudes (Tauxe *et al.* 2022; Figs 11–13).

In the PINT database, first, the data with ages between 0.05 and 2.6 Ma were filtered to focus on the Pleistocene period, which satisfyingly includes a high amount of data. Then, data obtained only

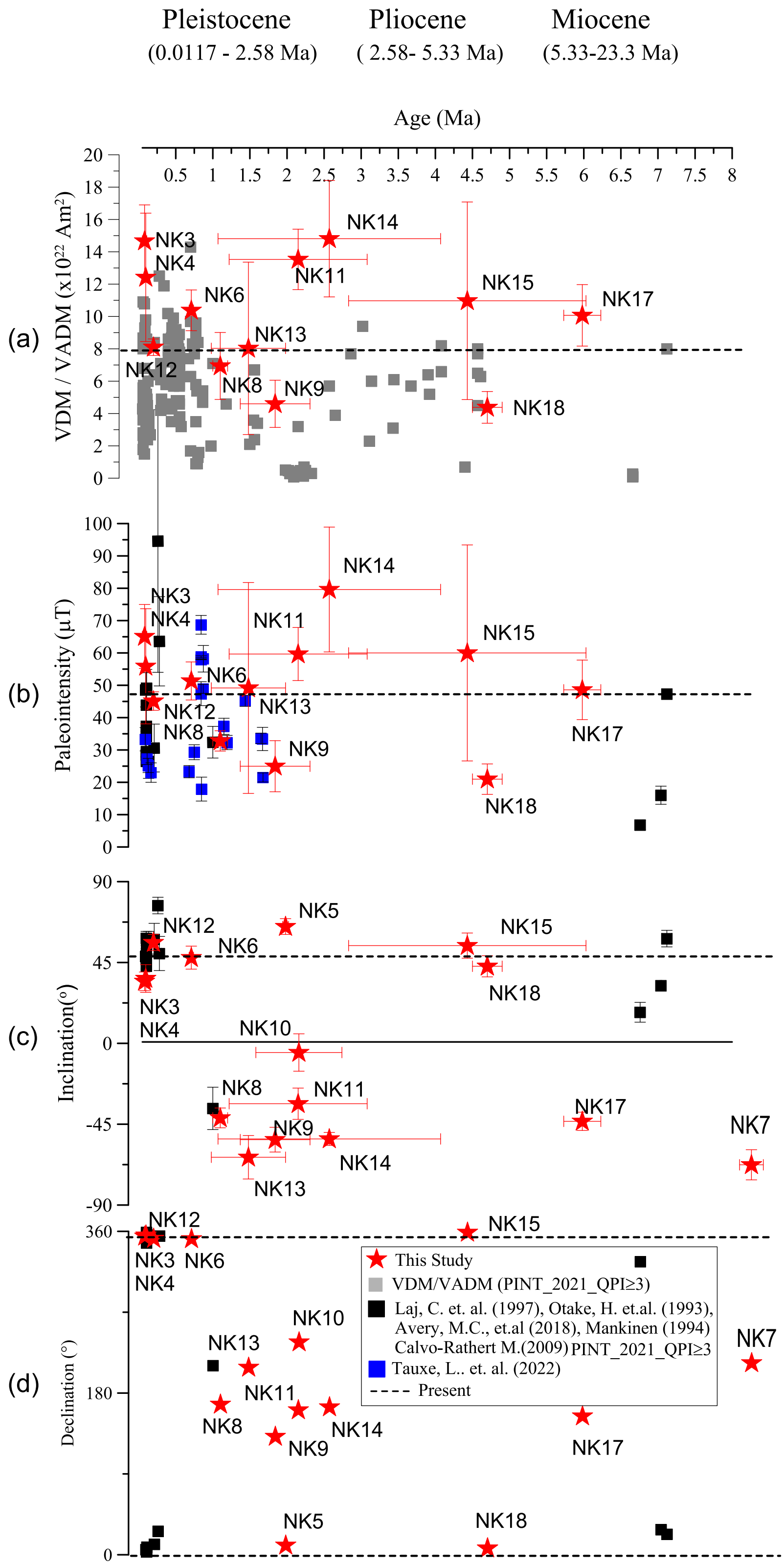

Figure 11. Virtual dipole moment (VDM), palaeointensity and palaeodirection results of samples from the study area. VDM, virtual dipole moment. VADM, virtual axial dipole moment.

with the Thellier-Thellier method (Thellier & Thellier 1959) (T+) and with QPI values more than 3 were chosen. The central Anatolia values (VADM of $10.3 \pm 3.7 \times 10^{22}$ Am^2) are higher than expected for a purely GAD field generated by a dipole with the present data value (7.7×10^{22} Am^2; Fig. 13). A comparison of our data with the averaged PINT data from 10° latitudinal bins and the globally averaged PADMs predicted from the PADM2M record shows that our results are higher than those two records (Figs 12a and 13). They

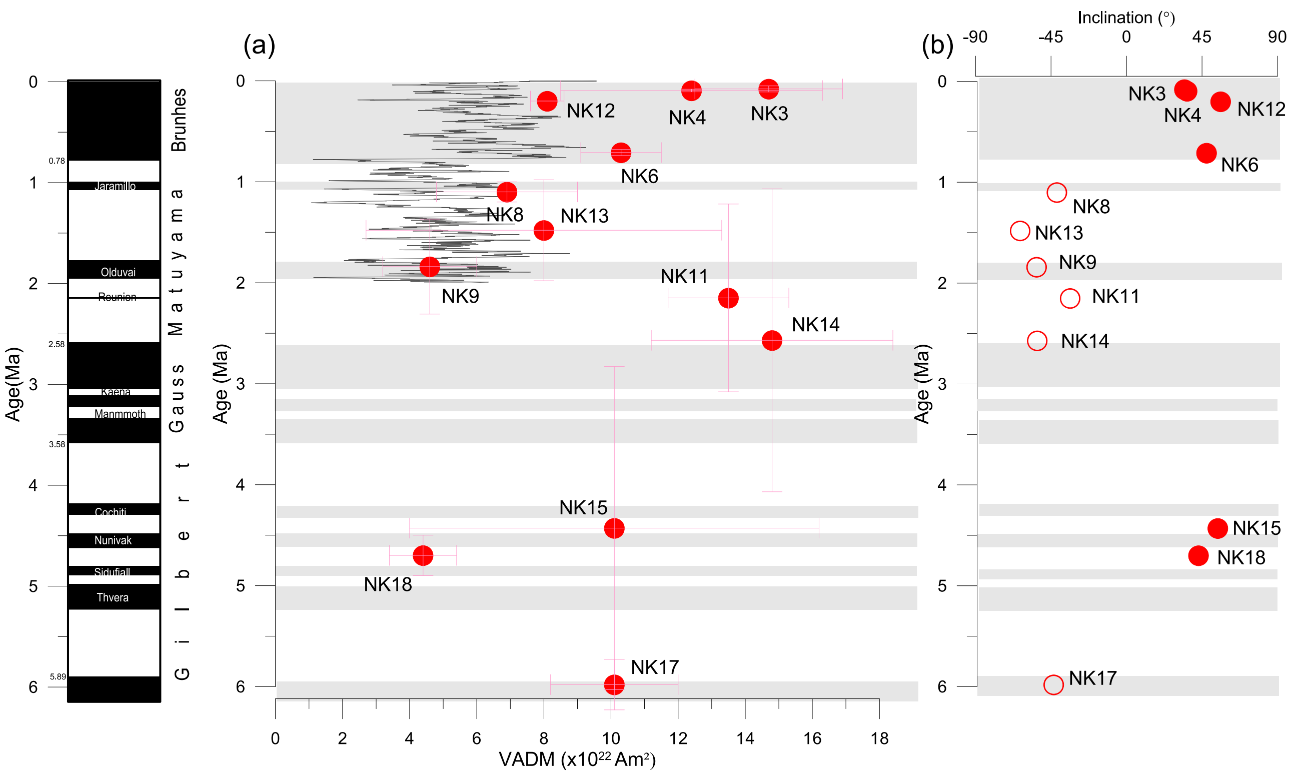

Figure 12. (a) VADM estimates for 0–6 Ma data from this study (red filled circles), globally averaged estimates from PADM2M of Ziegler *et al.* (2011) (grey line). (b) Inclination values obtained from the study (negative inclination: red empty circle; positive inclination: red filled circle. Magnetostratigraphy for 0–6 Ma Cande & Kent 1995).

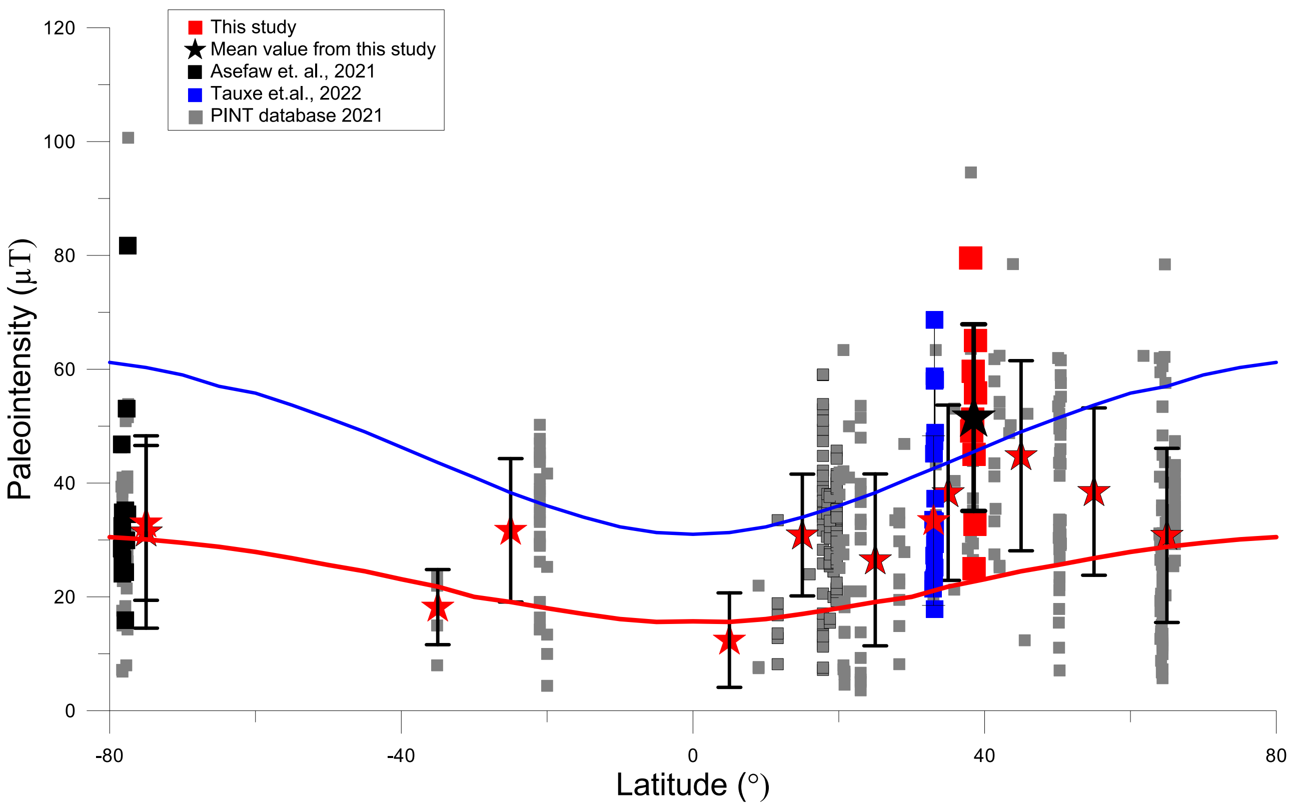

Figure 13. Palaeointensity data plotted against latitude median values for 10° bins (PINT database, Bono *et al.* 2021) and Asefaw *et al.* 2021; Tauxe *et al.* 2022 are shown as red stars. Estimated values for dipole moments of 80 ZAm^2 (present field) and 40 ZAm^2 (Tauxe *et al.* 2013; Cromwell *et al.* 2015; Asefaw *et al.* 2021) are shown as solid blue and dashed red lines, respectively.

are also on average slightly higher than Antarctica ($4.0 \pm 1.7 \times 10^{22}$ Am^2) and Northern Israeli values ($6.2 \pm 3.0 \times 10^{22}$ Am^2) estimated by Asefaw *et al.* (2021) and Tauxe *et al.* (2022), respectively.

Pleistocene results filtered from the PINT database and previous studies (Cromwell *et al.* 2015; Asefaw *et al.* 2021; Tauxe *et al.* 2022) suggest that data from mid-latitudes (Northern Hemisphere) are generally higher than those from the Southern Hemisphere or high northerly latitudes. This is also seen in field models for the Holocene (Constable *et al.* 2016), the average field for the last 100 ka (Panovska *et al.* 2018), and in the 5 Ma time average field (Cromwell *et al.* 2018), which all show asymmetry between the Northern and Southern Hemispheres. Our new data, which were the highest found for mid-latitudes in the Northern Hemisphere, significantly support this argument (Fig. 13).

6 CONCLUSIONS

We present 12 robust palaeointensity data estimated from lava from Central Anatolia from the Pleistocene (9 sites), Pliocene (2 sites) and upper Miocene (1 site) processed with the Thellier-type method. Previous studies sensitively dated the samples, except for one site which was dated in this study. The palaeointensity (VDM) value from the upper Miocene site (age 5.98 Ma) was estimated as 48.6 ± 9.2 μT ($10.1 \times 10^{22} \pm 1.9$ Am^2) which fitted well into the range of Neogene VDM values within data archives and had a higher value than obtained in a previous study performed on volcanic rocks from southeastern Spain by Calvo-Rathert *et al.* (2009). The palaeodirectional data clearly showed the Brunhes and Matuyama Chrons during the Pleistocene. Three robust data with 25.0 ± 7.9 μT (age 1.84 Ma), 59.7 ± 8.2 μT (age 2.15 Ma) and 79.6 ± 19.3 μT (age 2.57 Ma) during the early Pleistocene period, significantly contribute to global data archives, which have scarce palaeointensity data from a similar latitude range. Estimated palaeointensity values of Pleistocene age (0.71–1.48 Ma) from four sites are consistent with previous studies (Otake *et al.* 1993; Laj *et al.* 1997; Avery *et al.* 2018; Tauxe *et al.* 2022). For the Pliocene period, a palaeointensity (VDM) value of 21 ± 4.7 μT ($4.4 \pm 1.0 \times 10^{22}$ Am^2) with an age of 4.7 Ma was derived. The palaeomagnetic direction (D/I) of 7.4°/42.9° represents normal polarity field configuration. The low palaeointensity (VDM) value and the normal polarity likely place the obtained data in the Nunivak or Sidufjall normal polarity subchrons within the mostly reversed polarity Gilbert Chron. Previous studies show that low- to mid-latitude Northern Hemisphere field strengths are higher than the Southern Hemisphere due to asymmetry during the Pleistocene. To test this hypothesis, we compared our data with the palaeointensity (PINT) database (Bono *et al.* 2021), the PADM2M record (Ziegler *et al.* 2011) and previous studies (Constable & Korte 2006; Cromwell *et al.* 2013; Asefaw *et al.* 2021; Tauxe *et al.* 2022) during the Pleistocene. According to the comparison of our data, we concluded that the highest field strength obtained from Central Anatolia, which is located in the mid-latitude of the Northern Hemisphere, occurred due to asymmetry between the Northern and Southern Hemispheres during the Pleistocene.

ACKNOWLEDGMENTS

This work was supported by İstanbul University-Cerrahpaşa Scientific Research Foundationis a funding agency under Istanbul University-Cerrahpaşa (Project number: 25933). We would like to thank Melda Küçükdemirci, Niyazi Baydemir and Naci Orbay for their contribution to the manuscript and delightful discussion; and Özge Karslıoğlu Turgut, Nurullah Hanilçi and Namık Aysal for providing the optical microscope and their delightful discussions about the results. The authors also thank Manuel Calvo-Rathert and an anonymous reviewer, for their constructive comments, which have improved the manuscript, and Andrew Biggin for editorial handling.

DATA AVAILABILITY

The data underlying this paper are available in the paper and in its online supplementary material.

REFERENCES

Asefaw, H., Tauxe, L., Koppers, A.A.P. & Staudigel, H., 2021. Four-dimensional paleomagnetic dataset: plio-pleistocene paleodirection and paleointensity results from the Erebus volcanic province, Antarctica, *J. geophys. Res.*, **126**(2), 1–22.

Aubert, J., 2015. Geomagnetic forecasts driven by thermal wind dynamics in the Earth's core, *Geophys. J. Int.*, **203**, 1738–1751.

Avery, M.S., Gee, J.S., Bowles, J.A. & Jackson, M.J., 2018. Paleointensity estimates from ignimbrites: the Bishop Tuff Revisited, *Geochem. Geophys. Geosyst.*, **19**(10), 3811–3831.

Aydar, E., Çubukçu, H.E., Şen, E. & Akın, L., 2013. Central Anatolian Plateau, Turkey: incision and paleoaltimetry recorded from volcanic rocks, *Turkish J. Earth Sci.*, **22**(5), doi:10.3906/yer-1211-8.

Aydın, I., Karat, H.I. & Koçak, A., 2005. Curie-point map of Turkey, *Geophys. J. Int.*, **162**, 633–640.

Baydemir, N., Hisarlı, Z.M., Çinku, M.C., Keskin, M. & Kaya, N., 2012. Doğu Anadolu Bölgesi Kuvaterner yaşlı bazaltik kayaçlardan yermanyetik alan şiddetinin saptanması, İstanbul Yerbilimleri Dergisi, C.25, S.2, SS. 105–118.

Beekman, P.H., 1966. The Pliocene and Quaternary volcanism in the Hasan Dağ-Melendiz Dağ region, *Bull. Miner. Res. Explor. Inst. Turk.*, **66**, 90–105.

Besang, C., Eckhardt, F.J., Harre, W., Kreuzer, H. & Muller, P., 1977. Radiometrische Altersbestimmungen an Neogenen Eruptivgesteinen der Turkei, *Geol. Jb.*, **B.25**, 3–36.

Besse, J. & Courtillot, V., 2002. Apparent and True Polar Wander and the geometry of the geomagnetic field over the last 200 Myr, *J. geophys. Res.*, **107**, EPM 6–1-EPM 6-31.

Bigazzi, G., Yeğingil, Z., Ercan, T., Oddone, M. & Özdoğan, M., 1993. Fission track dating obsidians of central and northern Anatolia, *Bull. Volcanol.*, **55**, 588–595.

Biggin, A.J. & Paterson, G.A., 2014. A new set of qualitative reliability criteria to aid inferences on palaeomagnetic dipole moment variations through geological time, *Front. Earth Sci.*, **2**, 24, doi:10.3389/feart.2014.00024.

Bloxham, J., 1986. Evidence for asymmetry and fluctuation, *Nature*, **322**, 13–14.

Bono, R.K. *et al.*, 2021. The PINT database: a definitive compilation of absolute palaeomagnetic intensity determinations since 4 billion years ago, *Geophys. J. Int.*, **229**, 522–545.

Bucha, V. & Mellaart, J., 1967. Archaeomagnetic intensity measurements on some Neolithic samples from Çatal Hüyük (Anatolia), *Archaeometry*, **10**, 23–25.

Calvo-Rathert, M., Goguitchaichvili, A. & VegasTubia, N., 2009. A paleointensity study on middle Miocene to Pliocene volcanic rocks from southeastern Spain, *Earth Planets Space*, **61**, 61–69.

Cande, S. C. & Kent, D. V., 1995. Revised calibration of the geomagnetic polarity time scale for the Late Cretaceous and Cenozoic, *J. geophys. Res.*, **100**, 6093–6095.

Chadima, M. & Hrouda, F., 2006. *Remasoft 3.0 Paleomagnetic Data Browser and Analyzer*, Agico, Inc.

Channell, J.E.T., Xuan, C. & Hodell, D.A., 2009. Stacking paleointensity and oxygen isotope data for the last 1.5 Myr (PISO-1500), *Earth planet. Sci. Lett.*, **283**, 14–23.

Coe, R., 1967. The determination of paleointensities of the Earth's magnetic field with emphasis on mechanisms which could cause non-ideal behavior in Thellier's method, *J. Geomagn. Geoelectr.,* **19,** 157–179.

Coe, R.S., Gromme, S. & Mankinen, E.A., 1978. Geomagnetic paleointensities from radiocarbon-dated lava flows on Hawaii and thequestion of the Pacific nondipole low, *J. geophys. Res.,* **83,** 1740–1756.

Constable, C.G., Korte, M. & Panovska, S., 2016. Persistent high paleosecular variation activity in Southern Hemisphere for at least 10,000 years, *Earth planet. Sci. Lett.,* **453,** 78–86.

Constable, C. & Korte, M., 2006. Is Earth's magnetic field reversing?, *Earth planet Sci. Lett.,* **246,** 1–16.

Cromwell, G., Constable, C.G., Staudigel, H., Tauxe, L. & Gans, P.B., 2013. Revised and updated paleomagnetic results from Costa Rica, *Geochem. Geophys. Geosyst.,* **14,** 3379–3388.

Cromwell, G., Johnson, C.L., Tauxe, L., Constable, C.G. & Jarboe, N., 2018. PSV10: a global data set for 0–10 Ma time-averaged field and paleosecular variation studies, *Geochem. Geophys. Geosyst.,* **19,** 1533–1558.

Cromwell, G., Tauxe, L., Staudigel, H. & Ron, H., 2015. Paleointensity estimates from historic and modern Hawaiian lava flows using basaltic volcanic glass as a primary source material, *Phys. Earth planet. Inter.,* **241,** 44–56.

Day, R., Fuller, M. & Schmidt, V.A., 1977. Hysteresis properties of titanomagnetites: grain-size and compositional dependence, *Phys. Earth planet. Inter.,* **13,** 260–267.

Deenen, M.H.L., Langereis, C.G., van Hinsbergen, D.J.J. & Biggin, A.J., 2011. Geomagnetic secular variation and the statistics of palaeomagnetic directions, *Geophys. J. Int.,* **186,** 509–520.

Doell, R.R. & Dalrymple, G.B., 1966. Geomagneticp olarity epochsA: new polarity event and the age of the Brunhes-Matuyama boundary, *Science,* **152,** 1060–1061.

Doğan, U., 2011. Climate-controlled river terrace formation in the Kızılırmak Valley, Cappadocia section, Turkey: inferred from Ar-Ar dating of Quaternary basalts and terraces stratigraphy, *Geomorphology,* **126,** 66–81.

Dunlop, D.J., 2002. Theory and application of the Day plot (M_{rs}/M_s versus H_{cr}/H_c) 1. Theoretical curves and test using titanomagnetite data, *J. geophys. Res,* **107,** 2056.

Dunlop, D.J., 2011. Physical basis of the Thellier-Thellier and related paleointensity methods, *Phys. Earth planet. Inter.,* **187,** 118–138.

Engbers, Y.A., Grappone, J.M., Mark, D.F. & Biggin, A.J., 2022. Low paleointensities and Ar/Ar ages from Saint Helena provide evidence for recurring magnetic field weaknesses in the South Atlantic, *J. geophys. Res.,* **127,** e2021JB023358, doi:10.1029/2021JB023358.

Ercan, T., Tokel, S., Matsuda, J., Ul, T., Notsu, K. & Fujitani, T., 1992. New geochemical isotopic and radiometric data of the Quaternary volcanism of Hasandağı-Karacadağ (Central Anatolia), *TJK Bülteni,* **7,** 8–21 (In Turkish).

Ertepinar, P. *et al.*, 2020. Extreme geomagnetic field variability indicated by Eastern Mediterranean full-vector archaeomagnetic records, *Earth planet. Sci. Lett.,* **531,** 1–16.

Ertepinar, P., Langereis, C., Biggin, A. & De Groot, L., 2014. An archaeomagnetic study of Upper Mesopotamia and Central Anatolia between 2500 and 700 BCE. Further evidence for an extremely strong geomagnetic field ca. 3000 years ago, in *Proceedings of the EGU General Assembly Conference Abstracts,* held 27 April–2 May, 2014 in Vienna, Austria, id.9654.

Ertepinar, P., Langereis, C.G., Biggin, A.J., Frangipane, M., Matney, T., Ökse, T. & Engin, A., 2012. Archaeomagnetic study of five mounds from upper Mesopotamia between 2500 and 700 BCE: further evidence for an extremely strong geomagnetic field ca. 3000 years ago, *Earth planet. Sci. Lett.,* **357,** 84–98.

Finlay, C.C., Aubert, J. & Gillet, N., 2016. Gyre-driven decay of the Earth's magnetic dipole, *Nat. Commun.,* **7,** doi:10.1038/ncomms10422.

Fisher, R.A., 1953. Dispersion on a sphere, *Proc. R. Soc. Lond.,* **217**(1130), doi:10.1098/rspa.1953.0064.

Gubbins, D., Jones, A.L. & Finlay, C.C., 2006. Fall in Earth's magnetic field is erratic, *Science,* **312,** 900–902.

Innocenti, F., Mazzuoli, G., Pasquare, F., Radicati Di Brozolo, F. & Villari, L., 1975. The Neogene calcalkaline volcanism of Central Anatolia: geochronological data on Kayseri–Niğde area, *Geol. Mag.,* **112**(4), 349–360.

Kaya, N., 2020. The Variation of Geomagnetic Field Intensity in Central and Western Anatolia during Neogene-Quaternary, *PhD thesis,* Department of Geophysical Engineering, Institute of Graduate Studies, Istanbul University-Cerrahpasa, pp. 1–176, in Turkish.

Kirschvink, J.L., 1980. The least squares line and plane and the analysis of palaeomagnetic data, *Geophys. J. R. astr. Soc.,* **62,** 699–718.

Kissel, C. & Laj, C., 2004. Improvements in procedure and paleointensity selection criteria (PICRIT-03) for Thellier and Thellier determina-tions: application to Hawaiian basaltic long cores, *Phys. Earth planet. Inter.,* **147,** 155–169.

Korte, M., Constable, C., Donadini, F. & Holme, R., 2011. Reconstructing the Holocene geomagnetic field, *Earth planet. Sci. Lett.,* **312,** 497–505.

Korte, M. & Constable, C.G., 2005. The geomagnetic dipole moment over the last 7000 years-new results from a global model, *Earth planet. Sci. Lett.,* **236,** 348–358.

Krása, D., Heunemann, C., Leonhardt, R. & Petersen, N., 2003. Experimental procedure to detect multidomain remanence during Thellier-Thellier experiments, *Phys. Chem. Earth,* **28,** 681–687.

Laj, C., Guillou, H. & Kissel, C.A., 2014. Dynamics of the earth magnetic field in the 10–75 kyr period comprising the Laschamp and Mono Lake excursions: new results from the French Chaîne des Puys in a global perspective, *Earth planet. Sci. Lett.,* **387,** 184–197.

Laj, C., Rais, A., Surmont, J., Gillot, P.Y., Guillou., H., Kissel, C. & Zanella, E., 1997. Changes of the geomagnetic field vector obtained from lava sequences on the island of Vulcano (Aeolian Islands, Sicily), *Phys. Earth planet. Inter.,* **99,** 161–177.

Langel, R.A., 1987. Main field, in *Geomagnetism,* ed. Jacobs, J.A., Academic Press.

Le Pennec, J.L., Bourdier, J.L., Froger, J.L., Temel, A., Camus, G. & Gourgaud, A., 1994. Neogene ignimbrites of the Nevşehir plateau central Turkey: stratigraphy, distribution and source constraints, *J. Volc. Geotherm. Res.,* **63,** 59–87.

Leaton, B.R. & Malin, S.R.C., 1967. Recent changes in the magnetic dipole moment of the earth, *Nature,* **213,** doi:10.1038/2131110a0.

Leonhardt, R., Heunemann, C. & Krása, D., 2004a. Analyzing absolute paleointensity determinations: acceptance criteria and the software ThellierTool4.0, *Geochem. Geophys. Geosyst.,* **5**(12), doi:10.1029/2004GC000807.

Leonhardt, R., Krása, D. & Coe, R.S., 2004b. Multidomain behavior during Thellierpaleointensity experiments: a phenomenological model, *Phys. Earth planet. Inter.,* **147,** 127–140.

Leonhardt, R., Matzka, J. & Menor, E.A., 2003. Absolute paleointensities and paleodirections from Fernando de Noronha, Brazil, *Phys. Earth planet. Inter.,* **139,** 285–303.

Lisiecki, L.E. & Raymo, M.E., 2005. A Pliocene-Pleistocene Stack of 57 globally distributed benthic δ18O records, *Paleoceanography,* **20**(1), doi:10.1029/2004PA001071.

Liu, J., Nowaczyk, N.R., Panovska, S., Korte, M. & Arz, H.W., 2020. The Norwegian-Greenland sea, the laschamps, and the Mono Lake excursions recorded in a black sea sedimentary sequence spanning from 68.9 to 14.5 ka, *J. geophys. Res.,* **125**(8), doi:10.1029/2019JB019225.

Lovlie, R., 1989. Paleomagnetic stratigraphy: a correlation method, *Quater. Int.,* **1,** 129–149.

Lowrie, W., 1990. Identification of ferromagnetic minerals in a rock by coercivity and unblocking temperature properties, *Geophys. Res. Lett.,* **17,** 159–162.

Makaroğlu, Ö., Nowaczyk, N.R., Eriş, K.K. & Cagatay, M.N., 2020. High-resolution palaeomagnetic record from Sea of Marmara sediments for the last 70 ka, *Geophys. J. Int.,* **222**(3), 2024–2039.

Makaroğlu, Ö., 2021. A Holocene paleomagnetic record from Kucukcekmece Lagoon, NW Turkey, *Turk. J. Earth Sci.,* **30**(), 639–652.

Mankinen, E.A., 1994. Preliminary geomagnetic paleointensities from Long Valey Caldera, California, USGS Open-File Rep 94-633, Volcano Hazards Program.

McDonald, K.L. & Gunst, R.H., 1968. Recent trends in the Earth's magnetic field, *J. geophys. Res.,* **73,** 2057–2067.

MTA, 2013. *Türkiye Magmatik Kayaçlar Hartası,* Maden Tetkik Arama Genel Müdürlüğü (MTA), Ankara, Türkiye.

Mues-Schumacher & Schumacher, R., 1996. Problems of stratigraphic correlation and new K–Ar data for ignimbrites from Cappadocia, Central Turkey, *Int. Geol. Rev.,* **38,** 737–746.

Nagata, T., Arai, Y. & Momose, K., 1963. Secular variation of the geomagnetic total force during the last 5000 years, *J. geophys. Res.,* **68,** 5277–5282.

Nowaczyk, N.R., Frank, U., Kind, J. & Arz, H.W., 2013. A high-resolution paleointensity stack of the past 14 to 68 ka from Black Sea sediments, *Earth planet. Sci. Lett.,* **384,** 1–16.

Otake, H., Tanaka, H., Kono, M. & Saito, K., 1993. Paleomagnetic study of Pleistocene lavas and dykes of the Zao volcano group, Japan, *J. Geomagn. Geoelectr.,* **45,** 595–612.

Panovska, S., Constable, S.G. & Korte, M., 2018. Extending global continuous geomagnetic field reconstructions on timescales beyond human civilization, *Geochem. Geophys. Geosyst.,* **19,** 4757–4772.

Pasquarè, G., 1968. Geology of the Cenozoic volcanic area of Central Anatolia, *Atti Accad. Naz. Lincei,* **9,** 53–204.

Paterson, G.A., Tauxe, L., Biggin, A.J., Shaar, R. & Jonestrask, L.C., 2014. On improving the selection of Thellier-type palaeointensity data, *Geochem. Geophys. Geosyst.,* **15,** 1180–1192.

Platzman, H.S., Tapırdamaz, C. & Sanver, M., 1998. Neogene anticlockwise rotation of central Anatolia (Turkey) : preliminary paleomagnetic and geochronological results, *Tectonophysics,* **99,** 175–189.

Prèvot, M., Mankinen, E.A., Coe, R.S. & Grommè, C.S., 1985. The Steens Mountain (Oregon) geomagnetic polarity transition: 2. Field intensity variations and discussion of reversal models, *J. Geophys. Res.,* **90,** 10 417–10 448.

Reilinger, R.E. *et al.*, 1997. Global Positioning System measurements of present-day crustal movements in the Arabia–Africa–Eurasia plate collision zone, *J. geophys. Res.,* **102,** 9983–9999.

Riisager, P. & Riisager, J., 2001. Detecting multidomain magnetic grains in Thellier paleointensity experiments, *Phys. Earth planet. Inter.,* **125,** 111–117.

Saribudak, M. & Tarling, D.H., 1993. Archaeomagnetic studies of the Urartian civilization, eastern Turkey, *Antiquity,* **67,** 620–628.

Sayın, N. & Orbay, N., 2003. Investigation of secular variations of geomagnetic field using archaeomagnetic samples obtained from Central Anatolia, *İstanbul Üniv. Müh. Fak. Yerbilimleri Derg.,* **16**(1), 33–43.

Selkin, P. & Tauxe, L., 2000. Long-term variations in paleointensity, *Phil. Trans. R. Soc. Lond.,* **358,** 1065–1088.

Shaar, R. & Tauxe, L., 2013. Thellier GUI: an integrated tool for analyzing paleointensity data from Thellier-type experiments, *Geochem. Geophys. Geosyst.,* **14,** 677–692.

Singer, B.S., Guillou, H., Jicha, B.R., Zanella, E. & Camps, P., 2014. Refining the quaternary geomagnetic instability time scale (GITS): lava flow recordings of the blake and post-blake excursions, *Quat. Geochronol.,* **21,** 16–28.

Tarling, D.H., 1971. *Principles and Applications of Paleomagnetism*. Chapman and Hall.

Tauxe, L., Asefaw, H., Behar, N., Koppers, A.A.P. & Shaar, R. 2022. Paleointensity estimates from the Pleistocene of Northern Israel: implications for hemispheric asymmetry in the time averaged field, *Geochem. Geophys. Geosyst.,* **23**(9), doi:10.1029/2022GC010473.

Tauxe, L., Gee, J., Steiner, M. & Staudigel, H., 2013. Paleointensity results from the Jurassic: new constraints from submarine basaltic glasses of ODP Site 801C, *Geochem. Geophys. Geosyst.,* **14**(10), 4718–4733.

Tauxe, L., Kylstra, N. & Constable, C.,1991. Bootstrap statistics for paleomagnetic data, *J. geophys. Res.,* **96,** 11 723–11 740.

Tauxe, L. & Staudigel, H., 2004. Strength of the geomagnetic field in the Cretaceous Normal Superchron: new data from submarine basaltic glass of the Troodos Ophiolite, *Geochem. Geophys. Geosyst.,* **5**(2), doi:10.1029/2003GC000635.

Thellier, E. & Thellier, O., 1959. Sur l'intensite du champ magnetique terrestre dans le passe historique etgeologique, *Ann. Geophys.,* **15,** 285–376.

Toprak, V., 1998. Vent distribution and its relation to regional tectonics, Cappadocian Volcanics, Turkey, *J. Volc. Geotherm. Res.,* **85,** 55–67.

Valet, J.P., 2003. Time variations in geomagnetic intensity, *Rev. Geophys.,* **41,** 4/1–4/44.

Valet, J.P., Brassart, J., Le Meur, I., Soler, V., Quidelleur, X., Tric, E. & Gillot, P.Y., 1996. Absolute paleointensity and magnetomineralogical changes, *J. geophys. Res.,* **101,** 25 029–25 044.

Wardinski, I., Saturnino, D., Amit, H., Chambodut, A., Langlais, B., Mandea, M. & Thébault, E., 2020. Geomagnetic core feld models and secular variation forecasts for the 13th International Geomagnetic Reference Field (IGRF-13), *Earth, Planets Space,* **72,** 155, doi:10.1186/s40623-020-01254-7.

Yu, Y.J. & Tauxe, L., 2005. Testing the IZZI protocol of geomagnetic field intensity determination, *Geochem. Geophys. Geosyst.,* **6**(5), doi:10.1029/2004GC000840.

Ziegler, L., Constable, C., Johnson, C. & Tauxe, L., 2011. PADM2M: a penalized maximum likelihood model of the 0-2 Ma paleomagnetic axial dipole moment, *Geophys. J. Int.,* **184,** 1069–1089.

SUPPORTING INFORMATION

Supplementary data are available at *GJI* online.

NK_TDT.zip

Please note: Oxford University Press is not responsible for the content or functionality of any supporting materials supplied by the authors. Any queries (other than missing material) should be directed to the corresponding author for the paper.